Volume II

Appendix D.12

Impact Modeling

This appendix contains the independent analysis of the foam impact with the left wing conducted by Southwest Research Institute in support of the Columbia Accident Investigation Board. In addition to the analysis performed by NASA during the investigation, the Board called for a second independent analysis of the foam impact data. This report examines the foam impact data as it might have affected both thermal tiles and the RCC. The results of this analysis were used to predict damage to the RCC and tile and to set conditions for the foam impact testing program.

The conclusions drawn in this report do not necessarily reflect the conclusions of the Board; when there is a conflict, the statements in Volume I of the Columbia Accident Investigation Board Report take precedence.

Section 3.8 of CAIB Report Volume I, published in August 2003, states that details of impact tests performed during the investigation would be documented in Volume II, Appendix D.12. Due to the quantity of information required to describe this critical task, these details could not be included in this Volume. NASA Technical Publication TP-2003-212066, “Impact Testing of the Orbiter Thermal Protection System: Final Report in Support of the Columbia Accident Investigation,” to be released in December 2003, documents in detail the activities conducted by the Orbiter TPS Impact Test Team for the OVE Office, the NASA Accident Investigation Team, and the CAIB. The report is divided into six sections: (1) introduction, (2) test facility design and development, (3) test article and projectile fabrication, (4) test program descriptions, (5) results, and (6) future work. The report fully documents the test program development, methodology, results, analysis, and conclusions to the degree that future investigators can reproduce the tests and understand the basis for decisions made during the development of the tests. Furthermore, it will serve to communicate the results of the test program to decision makers, the engineering and scientific communities, and the public.

THIS PAGE INTENTIONALLY LEFT BLANK

APPENDIX D.12

Impact Modeling

Submitted by James D. Walker
Southwest Research Institute

EXECUTIVE SUMMARY

After the loss of the Orbiter *Columbia* during reentry on February 1, 2003, Southwest Research Institute (SwRI) was contracted by the Columbia Accident Investigation Board (CAIB) to perform impact modeling in support of the investigation. At the SwRI site, the CAIB in conjunction with the NASA Accident Investigation Team (NAIT) was performing impact tests against thermal protection system structures, including thermal tiles and fiberglass and reinforced carbon carbon (RCC) leading edges. To complement the extensive modeling work being carried out by the NAIT, the CAIB wished to support an independent analysis of the impact event.

Through the course of the work, SwRI developed a detailed analytic and numerical model of foam insulation impact on thermal tiles. This model provided a damage/no damage transition curve in the impact speed-impact angle plane. In particular, it was shown that the component of the foam impactor velocity that is normal to the impact surface determined whether there is tile damage. Thus, given an impact speed and an impact angle for an incoming piece of foam insulation, the model determined whether tile material would be damaged. This model agrees extremely well with previously performed tile impact work conducted at SwRI as well as with the tests performed during the Columbia accident investigation of foam insulation impacting tiles placed on the main landing gear door of Enterprise.

Computations were performed to examine the role of foam rotational velocity on the impact. Foam impactor rotational velocity can increase the damage done to tiles since it can increase the impact velocity component that is normal to the surface of the tile. An angle and impactor shape were determined that would produce similar damage to tile material as would the rectangular impactor with a given rotational velocity striking at the expected impact angle.

In addition to the modeling of tile, the impact of foam insulation on RCC panels was also modeled. Here, a numerical model was developed to model the panel and an analytic boundary condition was developed to model the pressure load supplied by the impacting foam. Once again, central to the load delivered and the stresses calculated is the normal component of the foam impact velocity. Comparison with the two tests performed against RCC panels led to estimates of failure stresses within the panel material. Parametric studies were performed with the model to investigate the question of impact location and to investigate the effect of foam impactors with rotational velocity. It was shown that a nonzero rotation velocity for the foam impactor nearly always increased the stresses on both the panel face and the rib of the panel. Computations were performed to determine the most severe loads within the framework of impact location and rotational velocities. Also, an estimate of an angle adjustment for a rotational velocity was determined, as actual tests did not include a rotating foam impactor.

In all, the modeling work was extremely successful and led to a greater physical understanding of the impact of foam insulation against the Orbiter's thermal protection system. In particular, it was shown that the most important piece of information is the velocity component of the foam that is normal to the surface being impacted. This velocity determines the loading stress on that surface. Given the stress, in the case of tiles, stresses above the crush-up stress lead to tile damage, while stresses below the crush-up stress lead to no damage. In the case of the RCC panel, the loading stress combined with the loading area gives rise to the loads seen by the panel and by the rib. These loads lead to stresses in both the panel and rib that subsequently can fail the rib or panel face. Though the geometry and deformation modes of the RCC panel do not produce a simple theory for damage as was found in the tile impact model, still the physical understanding of the impact is that stresses arise from normal velocities over a footprint of the impact to give loads that can then fail the panel.

SwRI appreciates the opportunity to participate in the Columbia investigation, and this report presents the work performed in the modeling effort.

THERMAL TILE AND FOAM INSULATION MODELS

To correctly model the impact of materials, it is essential to correctly model the materials involved. In order to do this, work began with the experimental testing of foam cubes left over from the 1999 SwRI testing program of foam against tile [1] and the testing of a thermal tile supplied by NASA.

The important information about both the foam and the tile that was lacking in the available data from NASA and the shuttle contractors was crush-up data for the material in compression. To address this lack of information, two 1" (2.54 cm)* cubes of tile left over from the 1999 SwRI testing program were crushed in an MTS test machine. The foam material is identified as NCFI 24-124 [1]. Two tests were performed. In the first, the foam was crushed till a large stress was reached, and in the second, three unload/reloads were performed during the crush up. Results are shown in Figs. 1 and 2. Strain rates were roughly 7×10^{-3}/s. The initial knee in the compression curve, where the slope of the stress-strain curve greatly diminishes, will be referred to as the "initial crush-up" and the corresponding stress will be referred to as the crush-up stress σ_{crush} in this report.

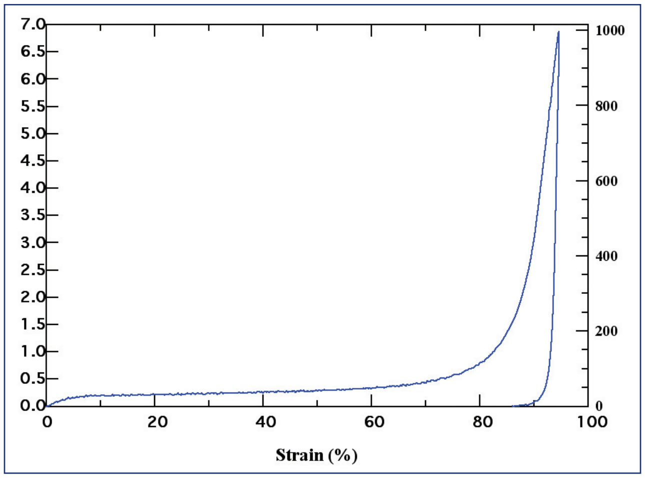

Figure 1. Results of test of foam cube.

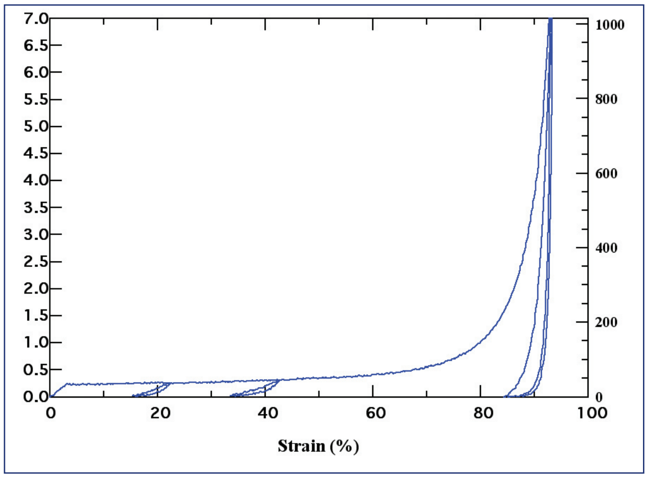

Figure 2. Test of second foam sample. Note the three unload/reloads.

Visual observation of the tests revealed two important facts about the foam during loading: first, there was virtually no lateral expansion; and second, when compressed the foam stayed intact and compressed (i.e., there was a permanent crush-up). The second observation on crush-up is confirmed in Figure 2 by the unloading curves that clearly indicate a permanent deformation.

However, in the tests that were being performed at SwRI under the NAIT/CAIB program with foam impacts against aluminum panels, it was clear that at the higher rates the foam was not permanently crushing up. It was undergoing large deformations, but after the impact it was releasing to its original shape.

Based on these observations, it was decided to model the foam as a nonlinear elastic material. Since impact computations were to be performed in the Eulerian hydrocode CTH from Sandia National Laboratories [2], it was important to develop the model in the context of CTH's computational algorithm. Within CTH, as with many hydrocodes, the material response is divided into a spherical response (i.e., a pressure-volume response) and a shear response. To correctly model the material, the fact that there was no lateral expansion of the material was caused by setting Poisson's ration ν equal to zero:

$$\nu = 0 \tag{1}$$

Within CTH, the local value of the shear modulus is computed from the current value of the bulk modulus and the constant Poisson's ratio. Thus, to model the material as a nonlinear elastic material with no lateral expansion, all that is required is determining the bulk response, that is, the bulk modulus as a function of pressure.

For a linear elastic material with a Poisson's ratio of zero, the bulk modulus K is simply 1/3rd the Young's modulus E, and the shear modulus G is simply 1/2 the Young's modulus:

$$K = E/3,\ G = E/2 \tag{2}$$

The initial values that were measured for the foam insulation at SwRI from the weight and dimensions of the samples and the stress-strain curves are given in Table 1. For a nonlinear elastic material with a Poisson's ratio of zero, corresponding differential relations between the local bulk modulus, shear modulus and Young's modulus apply. Thus, specifying one of the moduli as a function of pressure and energy completely determines the elastic response.

	ρ_0	E_0	σ_{crush}	ν
Foam Insulation	0.03844 g/cm^3 2.4 lb/ft^3	8.0 MPa 1160 psi	220 kPa 31.9 psi	0
Tile	0.18 g/cm^3 11.2 lb/ft^3	27.0 MPa 3916 psi	345 kPa 50 psi	0

Table 1. Measured Properties of the Foam Insulation and the Thermal Tile.

Within CTH, new subroutines were written to model the foam insulation and thermal tile material response. Some details of these routines are described in another portion of the Columbia Accident report since CTH is an Export Controlled code. The model essentially returned the pressure and bulk modulus given a density. The table of values from which the subroutine linearly interpolated to produce pressures and moduli (in particular, the local bulk sound speed) for the foam insulation is given in Table 2. Since these are axial stress values, they correspond to the Young's modulus, and the corresponding bulk modulus was found by dividing by 3. Also, no thermal component to the stress was included in the EOS. Thus, given the density of the material, its pressure state was determined. The final values with very large stresses are to provide robustness to the computational scheme so that, if large compressions did occur, the EOS would be able to provide corresponding pressures.

Density	Axial Stress	Density (g/cm^3)	Axial Stress (kPa)
0 g/cm3	0 Pa	0.	0
$0.3\times\rho_0$	$-2\sigma_{crush\text{-}f}$	0.015320	-440
$(1-\sigma_{crush\text{-}f}/E_{0f})\rho_0$	$-\sigma_{crush\text{-}f}$	0.037383	-220
ρ_0	0 Pa	0.038440	0
$(1+\sigma_{crush\text{-}f}/E_{0f})\rho_0$	$\sigma_{crush\text{-}f}$	0.039497	220
$\rho_0/0.3$	$2\sigma_{crush\text{-}f}$	0.128133	440
$\rho_0/0.15$	1.31 MPa	0.256267	1.31×10^3
$\rho_0/0.05$	7 MPa	0.768800	7.00×10^3
$\rho_0/0.04$	7 GPa	0.961000	7.00×10^6

Table 2. Tabular Foam Insulation Values in EOS.

Due to the tests with the foam showing no permanent crush-up during the dynamic tests, the foam was modeled as purely elastic by 1) setting a flag within the new EOS to say that the pressure response was elastic (i.e., there was no permanent crush-up) and 2) setting the yield stress in the elastic-plastic portion of the code to 7 MPa (~1 ksi). It is unlikely this stress level will be reached, so this stress is viewed as a large stress to maintain elastic behavior in the foam. Also required within CTH is a tensile failure stress which was set to 230 kPa (33.4 psi).

For the foam insulation, Figure 3 compares the model to the data from the two tests, and Figure 4 is an enlargement of the low pressure region. The agreement is excellent.

Similar material characterization work was performed on a shuttle thermal tile. SwRI was mailed a tile (MISC-794-400-120) from which were cut roughly 2" (5.08 cm) cube samples. Two cubes were then crushed in an MTS machine. The results of the crushing are shown in Figs. 5 and 6. Strain rates were roughly 3×10^{-3}/s.

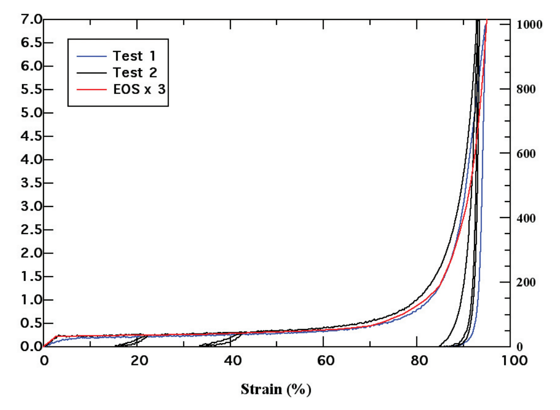

Figure 3. Stress-strain curve for foam: blue and black from tests, red from model.

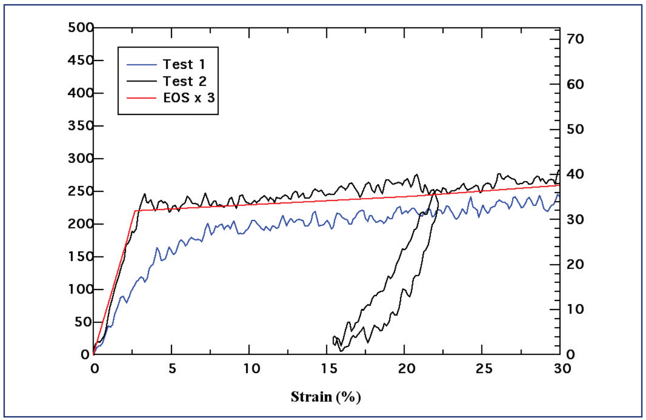

Figure 4. Enlargement of stress-strain curve for foam in Figure 3: blue and black from tests, red from model.

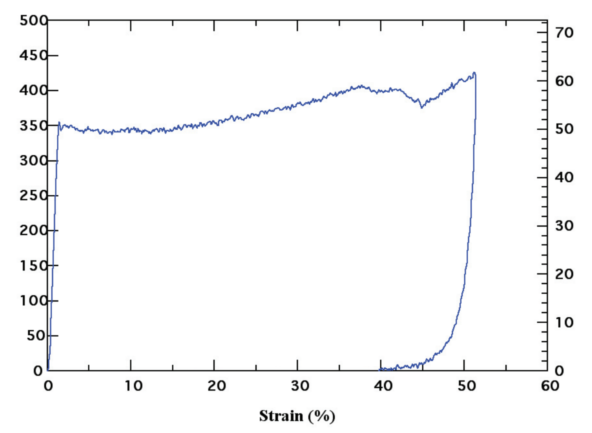

Figure 5. Stress-strain curve for shuttle thermal tile.

The initial values (i.e., near zero stress) that were measured for the thermal tile at SwRI from the weight and dimensions of the samples and the stress-strain curves are given in Table 1. Though it is clearly an LI-900 tile, the measured density was larger than the stated 9 lb/ft^3. As throughout this report, the values measured at SwRI will be used in the modeling and analysis.

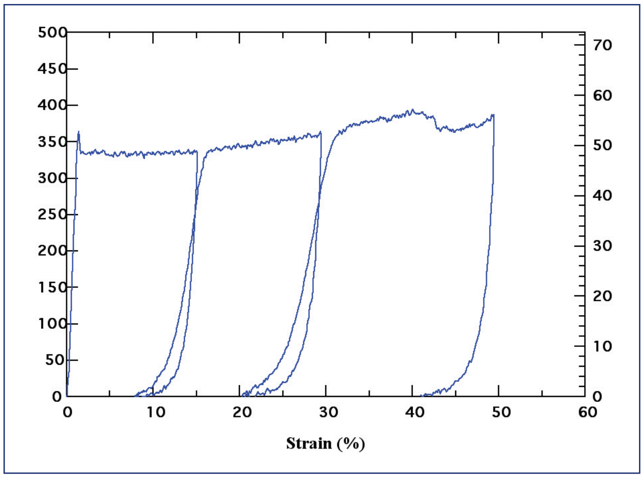

Figure 6. Stress-strain curve for shuttle thermal tile, including unload/reloads.

Upon loading, the initial crush-up point in the curve occurs at 345 kPa (50 psi). After this point, there is a slowly increasing stress as strains increase. A difference between the foam crush-up and the tile crush-up is that the tile breaks apart. Visual observation during the compression test indicated that failure begins when the stress-strain curve begins to dip in the 40% strain region. Fractures form in the tile material and the cube of tile subsequently disintegrates as loading progresses. To model this behavior, the elastic-plastic yield stress was set to 400 kPa (58 psi). The elastic-plastic yield is an important part of the crush-up behavior of the tile (see Figure 8, where the solid curve is without the yield stress while the dot-dash curve is with the yield stress in the formulation). Also, a failure model was invoked, namely that the material would fail at 50% equivalent plastic strain (this failure model was invoked by using constants D2=0.5, D1=D3=D4=D5=0 in the Johnson-Cook fracture model). The tensile failure stress was set at 360 kPa (52.2 psi). Also important in the computations that included both foam and tile was setting certain parameters in the CTH fracture input: pfvoid=pffrac=-50 kPa and setting nface1 and nface2 equal to the material numbers of the foam and tile. Though the tensile behavior is not well modeled (a general problem for Eulerian codes), it is an important part of the model and does affect results. Fortunately, the most interest for these models is when the materials are under compression.

For the tile model, permanent crush up was assumed to occur. Thus, once compressed beyond the crush-up stress, a permanent set occurs and the unloading curve is different than the loading curve. This behavior was accomplished by setting the appropriate flag in the new EOS model in CTH.

The model for the thermal tile material is shown in comparison to test data in Figs. 7 and 8. The behavior beyond the failure of the tile material is extrapolated based on the foam's properties. Table 3 displays the values of axial stress versus the density, similar to Table 2 for foam. This table, with the Poisson's ratio equal to zero and the yield stress and fracture model as defined above, completely defines the material response.

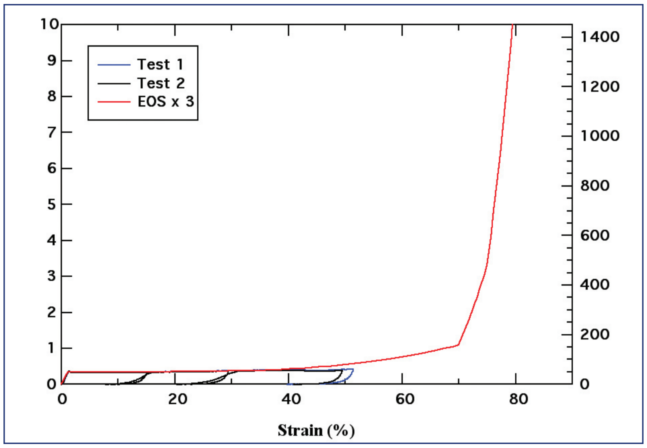

Figure 7. Stress-strain curve for thermal tile: blue and black are data, red is model.

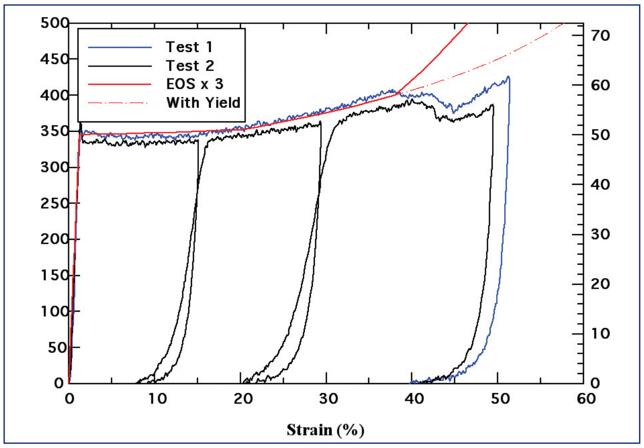

Figure 8. Enlargement of tress-strain curve for thermal tile: blue and black are data, red is model (solid curve is without yield; dashed curve is behavior with yield).

Density	*Axial Stress*	*Density (g/cm³)*	*Axial Stress (kPa)*
0 g/cm³	0 Pa	0.	0
$0.3\times\rho_0$	$-2\sigma_{crush\text{-}t}$	0.0540	-690
$(1-\sigma_{crush\text{-}t}/E_{0t})\rho_0$	$-\sigma_{crush\text{-}t}$	0.1777	-345
ρ_0	0 Pa	0.1800	0
$(1+\sigma_{crush\text{-}t}/E_{0t})\rho_0$	$\sigma_{crush\text{-}t}$	0.1823	345
$\rho_0/0.8$	352 kPa	0.2250	352
$\rho_0/0.62$	400 kPa	0.2903	400
$\rho_0/0.50$	550 kPa	0.3600	550
$\rho_0/0.30$	1.10 MPa	0.6000	1.10×10^3
$\rho_0/0.25$	3.30 MPa	0.7200	3.30×10^3
$\rho_0/0.20$	11.0 MPa	0.9000	1.10×10^4
$\rho_0/0.18$	11.0 GPa	1.0000	1.10×10^7

Table 3. Tabular Tile Values Used in EOS.

FOAM IMPACT ON TILE COMPUTATIONS

The models developed above were then exercised by examining the impact tests reported in [1]. These tests included 1" (2.54 cm) cubes of foam insulation impacting individual thermal tiles at various angles and velocities. The experiments included impacts ranging from no-damage to significant damage to and cratering in the tiles, and were thus viewed as a good range of data to compare against.

Most of the computations were performed in 2-dimensional plane strain. It turned out that due to the physics involved (and as was explicitly shown for one case), there was excellent agreement between 3-dimensional and 2-dimensional calculations for the impact parameters considered. Computations were performed with CTH for a variety of striking angles and velocities. Information extracted from the computations primarily focused on the normal stress at the surface of the tile; the histories of these stresses were examined at locations spaced 0.5 cm apart on the tile surface.

As a first example, the comparison between a 2D and 3D computation will be considered. Figure 9 shows the initial geometry for both the 2D and 3D computation. The thermal tiles are 6" × 6" × 2" in 3D, and 6" × 2" in 2D. The impact velocity was chosen to be 800 ft/s (244 m/s) at a striking angle of 30°. The cell size in the computations was 1 mm cube or square, depending on the dimension, with 160 × 100 × 40 cells used in 3D (a plane of symmetry was assumed at the center, and only 1.5" width of the half tile was included), and 160 × 100 cells used in 2D. The computations were carried out to 500 μs. The figure also shows frames of each computation at 200 and 500 μs. The outlines of the materials show that the deformation in these cases is quite similar. The colors in the figures show σ_{yy} , where y is the vertical axis. Though similar, it can be seen that the stresses away from the impact region are lower in the 3D computation as the extra dimension has stress-free boundaries that supply rarefaction waves reducing the stress beneath the impact site.

As a quantitative measure, results from the experiment as well as the computations are shown in Table 4. The final crater dimensions agree very well for the three cases. In addition to considering the final crater dimensions, the normal stress (σ_{yy}) histories at 0.5 cm interval locations were compared (Figure 10). As can be seen, the normal stress histories agree very well for the two computations. Due to the agreement, further calculations to explore the behavior of the impact event were carried out in 2D plane strain.

	Crater Depth	Crater Length	Crater Width
Experiment [1]	0.64 cm (0.25")	5.1 cm (2")	3.2 cm (1.25")
3D computation	0.8 cm (0.3")	6.4 cm (2.5")	2.9 cm (1.15")
2D computation	0.8 cm (0.3")	5.4 cm (2.1")	n/a

Table 4. Comparison Between Experiment and 3D and 2D-Plane-Strain Computations.

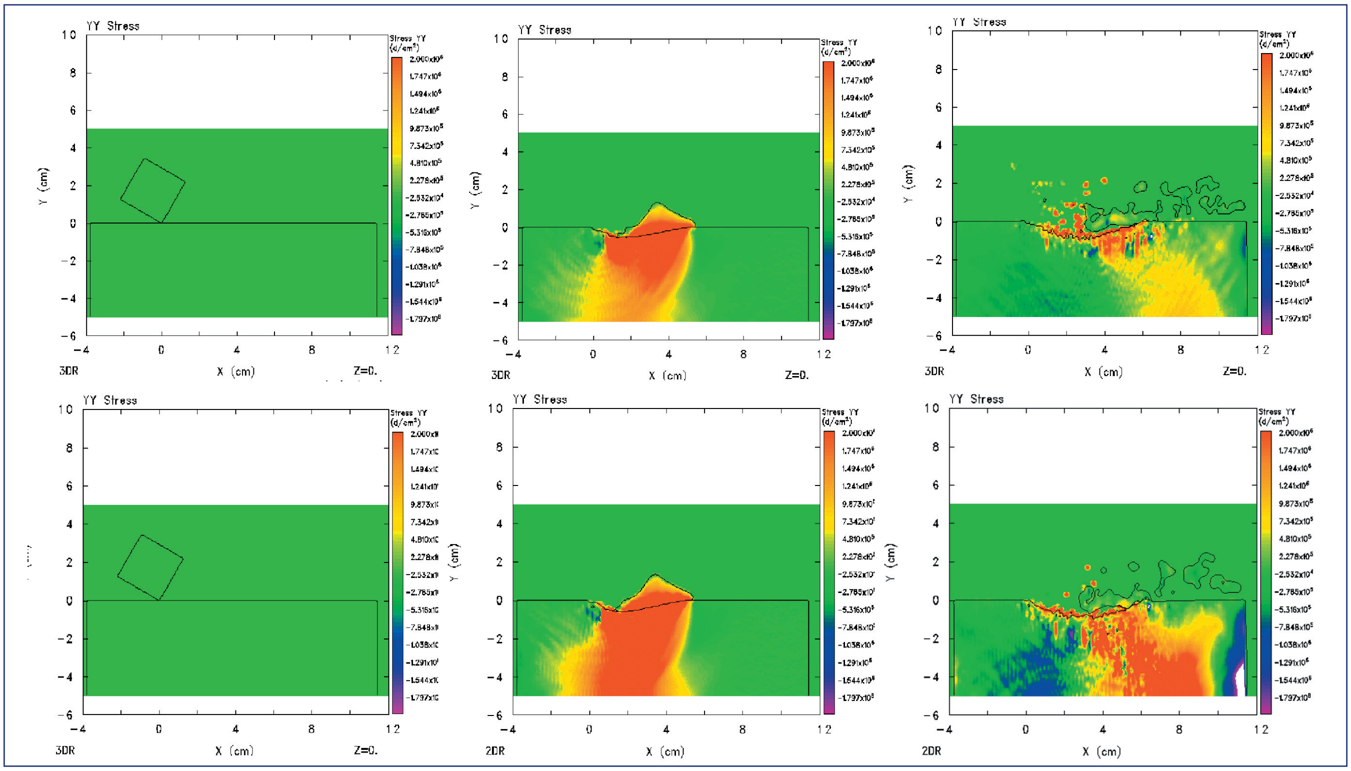

Figure 9. CTH computations with new foam insulation and thermal tile models. Top is 3D computation, bottom is 2D plane strain of 1" cube of foam insulation material impacting thermal tile at 800 ft/s at 30° impact angle. Times are 0, 200 and 500 μs. Colors mark σ_{yy}, ranging from –200 kPa (-29 psi, purple) to 200 kPa (red); green is 0 kPa.

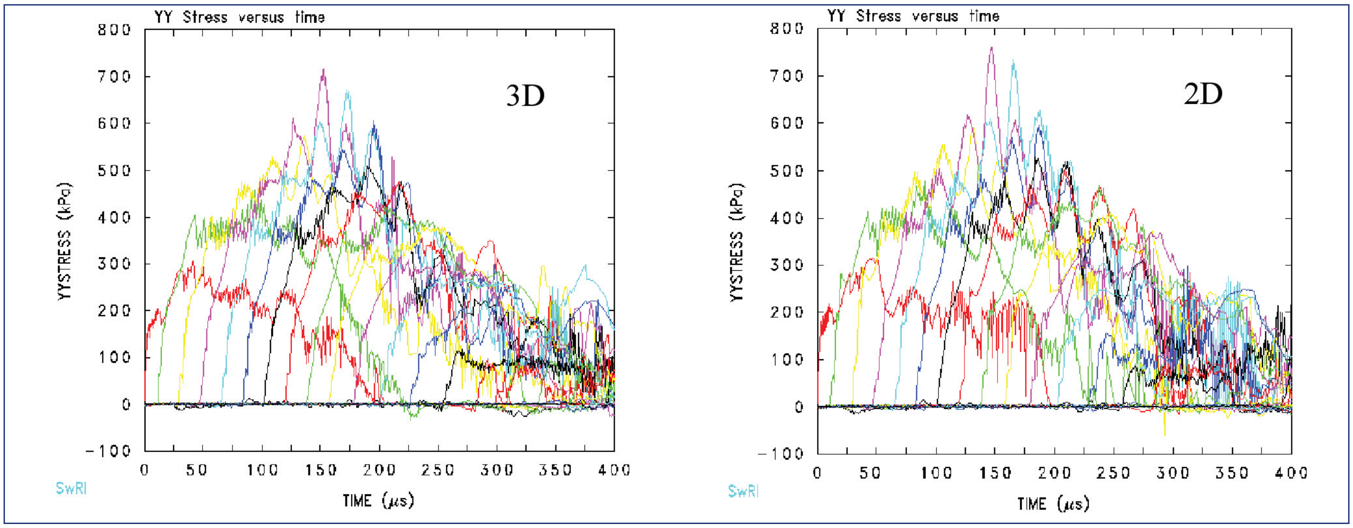

Figure 10. Normal stress histories for 3D (left) and 2D-plane-strain (right) computations of 1″ cube of foam insulation impacting thermal tile at 800 ft/s at 30° impact angle.

Damage/No Damage Criteria

Given that the material models and impact simulations were behaving well and reproducing experimental results, it was decided to pursue a damage/no damage transition curve through computation. In particular, a sequence of computations was performed with the intent of determining whether an impacting 1” cube of foam insulation material would damage the thermal tile. The damage/no damage decision was based on an examination of both the final state of the tile surface and the normal stress history at the gage locations along the tile surface. For example, the computation at 700 ft/s at 15° impact angle was decided to have no damage since there was little deformation at the surface of the tile (what deformation is seen there is typical of numerical anomalies in interfaces in Eulerian codes) and the stresses remain below the 345 kPa (50 psi) crush-up stress determined above for the thermal tiles. The results are shown in Figure 11.

However, for an impact at the same velocity but a larger impact angle, damage does occur. Figure 12 shows the results for 1” cube of foam insulation impacting a thermal tile at 700 ft/s at a 23° impact angle. In this case there is damage: a crater is seen when the surface of the tile is examined and the normal stresses at the interface exceed 345 kPa by a significant amount and for a significant time duration.

Mapping Out the Damage/No Damage Transition Curve

A series of computations were performed to determine the damage/no damage transition curve in the impact speed-impact angle plane. In each case a given impact speed and impact angle computation was performed with the new model in CTH, and based on the arguments presented above either “damage” or “no damage” (or in some in-between cases, “slight damage”) was assigned to the results. These

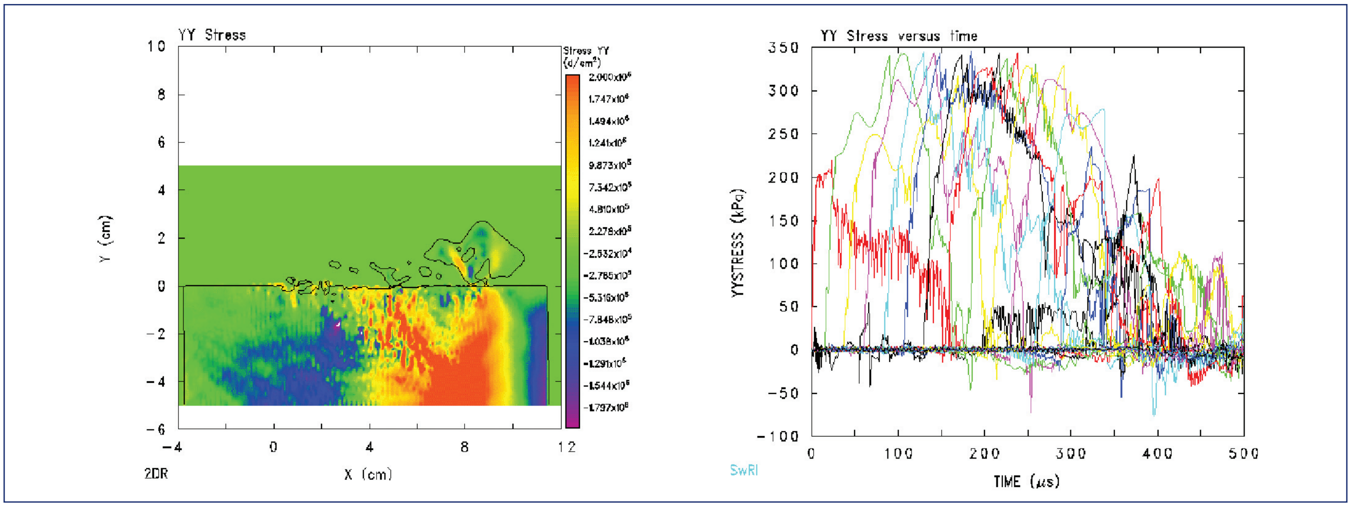

Figure 11. σ_{yy} (left) and normal stress (σ_{yy}) histories (right) for 1″ cube of foam insulation impacting thermal tile at 700 ft/s at 15° impact angle; no damage occurs to the tile.

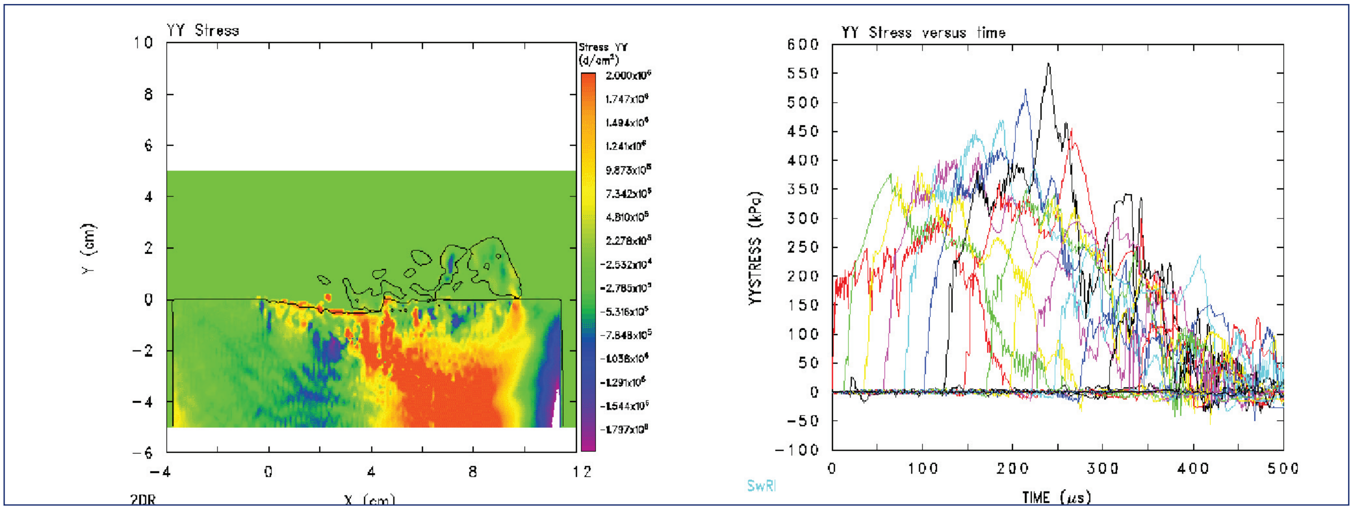

Figure 12. σ_{yy} (left) and normal stress (σ_{yy}) histories (right) for 1″ cube of foam insulation impacting thermal tile at 700 ft/s at 23° impact angle; damage occurs to the tile.

computations were then plotted in the impact speed-impact angle plane. After each computation, the decision was made on what case to run next, thus allowing the curve to be followed. Table 5 shows the results of the computations. When plotted on a graph, these results give indication of a fairly well defined damage/no damage transition curve in the plane (Figure 13).

Velocity (ft/s)	No Damage	Slight Damage	Damage
175	40°, 50°, 70°		
200	90°	40°, 50°, 70°	
225		50°	
250		50°, 90°	
300	30°		90°
400	20°, 25°		30°
500	20°	25°	30°
600	17°	20°, 23°	25°
700	10°, 15°		20°, 23°, 30°
800	13°	17°	20°
900	12°		17°
1000	10°	15°	20°
1100	10°		15°
1200	10°		15°
1400	10°		13°
1600	7°	10°	12°

Table 5. Results of Computations of 1″ Cube of Foam Insulation Impacting a Thermal Tile. Each Angle Entry Represents a CTH Calculation.

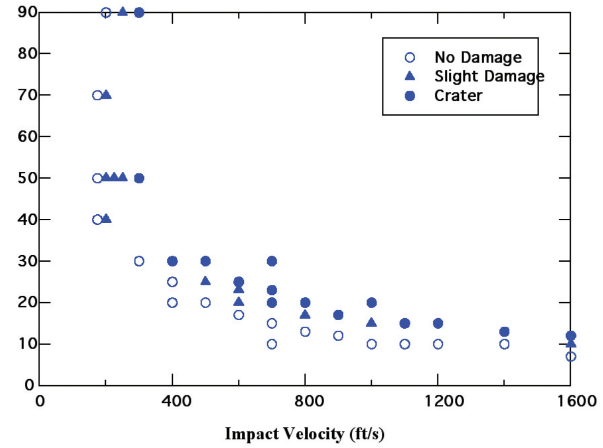

Figure 13. Damage/no damage results from numerical calculations.

Analytical Model for Damage/ No Damage Transition Curve

When the foam insulation material impacts the tile surface at an angle, it appears it is possible to separate the velocity of the foam material into two parts: tangential to the surface and normal to the surface. As there is no Poisson's effect for the foam, the two behaviors seem to separate nearly completely. Thus, the question arises as to what normal velocity leads to the crush-up of the thermal tile. The Hugoniot jump conditions for mass and momentum conservation for a shock moving to the right state

$$\rho_2 = \frac{\rho_1}{1 - \dfrac{u_2 - u_1}{U - u_1}} \tag{3}$$

$$\sigma_2 - \sigma_1 = \rho_1(U - u_1)(u_2 - u_1) \tag{4}$$

where subscript 1 refers to the region in front of the shock (before passage) and subscript 2 refers to the region behind the shock, U is the shock velocity, ρ is density, σ is stress and u is particle velocity. For the impact situation here, the crush-up stress of the foam insulation is less than that of the tile and therefore the foam will achieve its crush-up stress and then continue loading into its relatively flat stress-response region (Figure 4). The thermal tile, on the other hand, will be responding in its initial elastic regime up to the crush-up stress. In equations for each material, with the subscript e referring to elastic, the material states after the passage of the initial elastic wave are

$$\rho_e = \frac{\rho_0}{1 - \dfrac{u_e}{c_0}} \qquad (5)$$

$$c_0 = \frac{\sigma_{crush}}{\rho_0 c_0} \qquad (6)$$

where subscript 0 refers to the initial state and $c_0 = \sqrt{(E_0/\rho_0)}$ (the Young's modulus is used in this expression for the longitudinal sound speed since Poisson's ratio is zero). At the crush-up stress of the thermal tile, the material velocity in the tile is u_{et} and the stress is $\sigma_{crush\text{-}t}$ (where the subscript t stands for tile). The Hugoniot jump conditions are now applied to the foam insulation to give

$$\sigma_{crush\text{-}t} - \sigma_{crush\text{-}f} = \rho_{ef}\,(c_{1f} + u_{ef})(V_{crush} - u_{ef} - u_{et}) \qquad (7)$$

Solving for the impact velocity at which the tile crush stress is reached yields

$$V_{crush} = u_{et} + u_{ef} + \frac{\sigma_{crush\text{-}t} - \sigma_{crush\text{-}f}}{\rho_{ef} = (c_{1f} - u_{ef})} \qquad (8)$$

This equation for the crush velocity can be evaluated using the properties of the foam insulation and thermal tile material determined above. The values obtained are

c_{0f} = 456 m/s
c_{0t} = 387 m/s
c_{1f} = 49.8 m/s
ρ_{ef} = 0.03953 g/cm^3
ρ_{et} = 0.18233 g/cm^3
u_{ef} = 12.5 m/s
u_{et} = 4.95 m/s
V_{crush} = 68.2 m/s (224 ft/s)

Thus, for a normal impact of foam insulation against a thermal tile, crush-up of the thermal tile begins at an impact velocity of 68.2 m/s. This derivation was for one-dimensional response. In the situation where the piece of foam is impacting at an angle θ, the normal velocity (the velocity into the tile) is given by

$$V_y - V\sin(\theta) \qquad (9)$$

Thus, for foam insulation impacting thermal tile at a velocity V and angle θ, the thermal tile will begin to crush at

$$V - V_{crush}/V\sin(\theta) \qquad (10)$$

For the value of V_{crush} computed for the foam insulation impact into tile, this damage/no damage transition curve is plotted in Figure 14 along with the results from the computations. It is seen that there is excellent agreement.

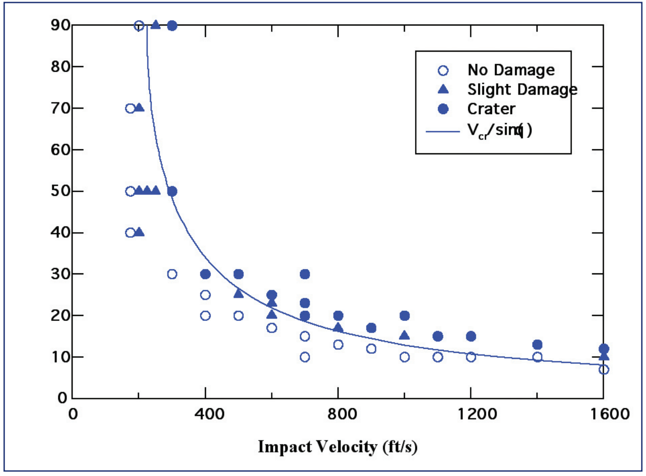

Figure 14. Theoretical damage/no damage transition curve with computational results.

Returning to the reports of previous work performed at SwRI [1,3], all the experimental results of foam insulation impact into single thermal tiles were categorized with the same damage/slight damage/no damage designation. Figure 15 breaks out these various impact cases. Figures 15a-c are for NCFI 24-124 [1]. The material in Figure 15d from [3] is an ablator material with a higher density (around 0.3 g/cm^3, 19 lb/ft^3) and unknown crush strength.* Rough dimensions of the impactors are shown in the figure captions. Of most interest are the foam insulation impactors with leading cross section 1" × 1" (Figure 15a). Though of two different lengths, the agreement is remarkable. In this case, the tile is fully loaded by the foam, and the length of the impactor does not affect whether damage occurred (it does affect crater size [1]). In other cases with much smaller cross sections, it is likely the projectile buckled before fully loading the tile, thus leading to less damage to the tile. Figure 15e shows results of tests performed during the Columbia investigation (discussed below). Finally, Figure 15f shows all the data points plotted with the theoretical curve. The agreement is excellent.

A strong case can be made that the foam insulation impacting thermal tiles is well understood. Good agreement has been shown between the large-scale numerical computations, the theoretical model, and experimental results. Thus, it is clear that loading from the foam arises from the component of the velocity normal to the surface being struck. If the resulting normal stress exceeds the crush-up stress of the tile, then the thermal tile crushes and a crater is formed. Otherwise, there is minimal or no damage to the tile. Figure 16 puts all three (CTH calculations, theoretical curve, experimental results) on one plot.

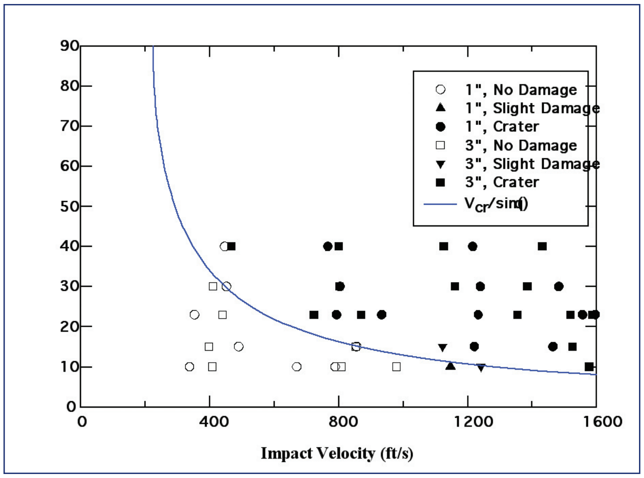

Figure 15a. 2.54 × 2.54 × 2.54/7.62 cm.

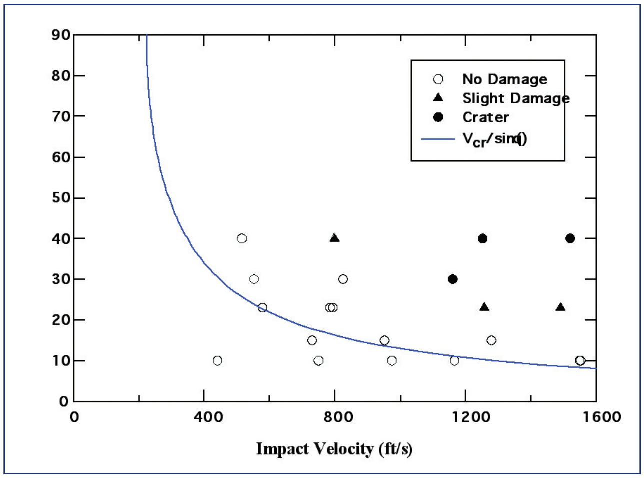

Figure 15b. 0.64 x 2.3 x 2.3 cm.

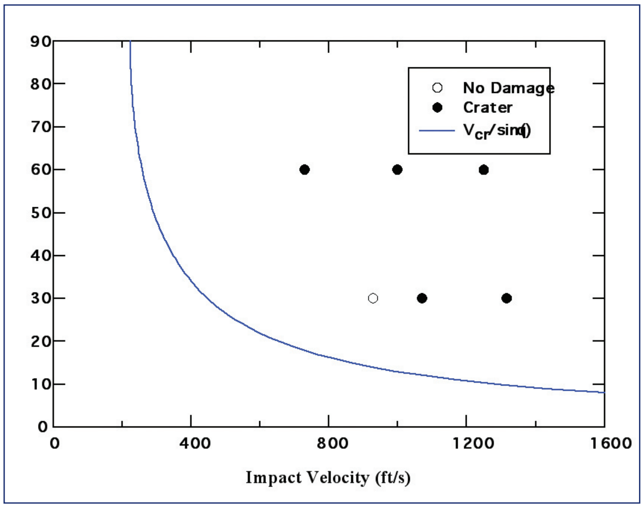

Figure 15c. 0.95 diameter x 7.62 cm.

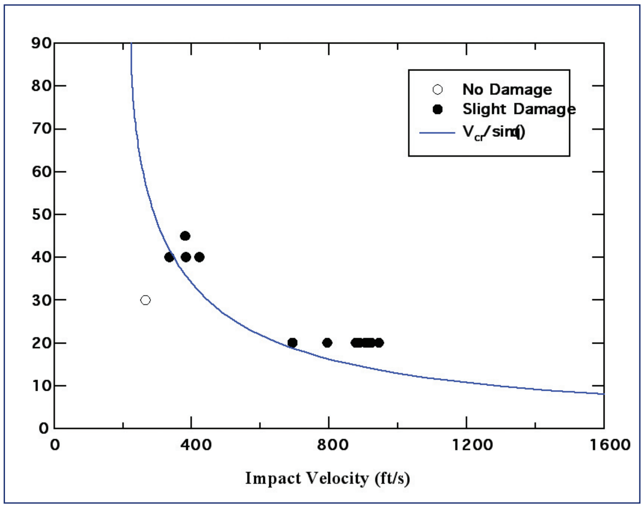

Figure 15d. 0.5 x 0.5 x 5.1 cm (ablator) [3].

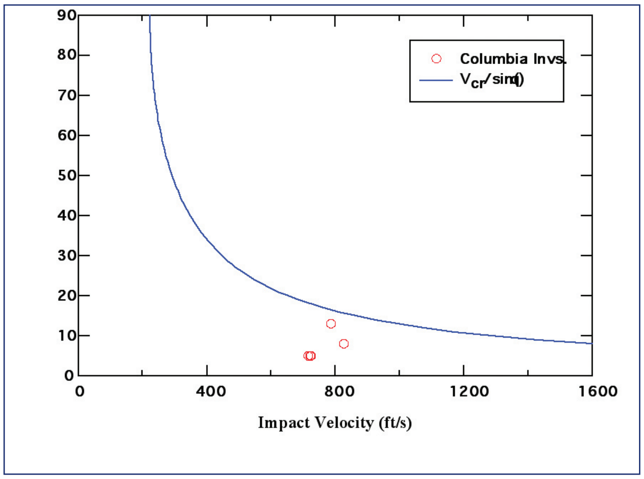

Figure 15e. Columbia investigation tests.

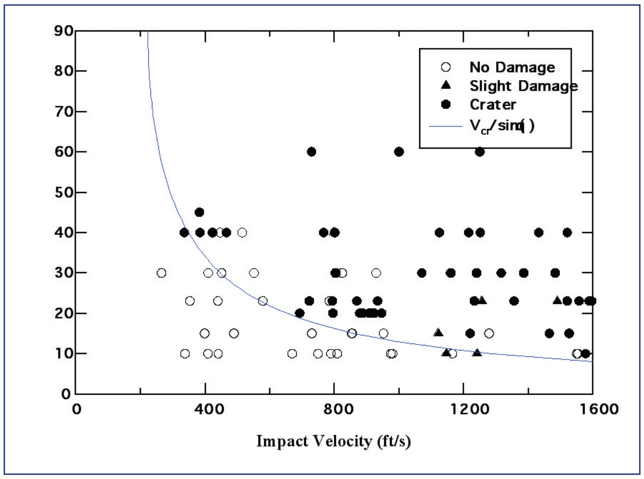

Figure 15f. All data from [1] and [3].

Figures 15a – 15f. Theoretical damage/no damage transition curve with results of all impacts into thermal tiles contained in [1,3] and Columbia investigation tests.

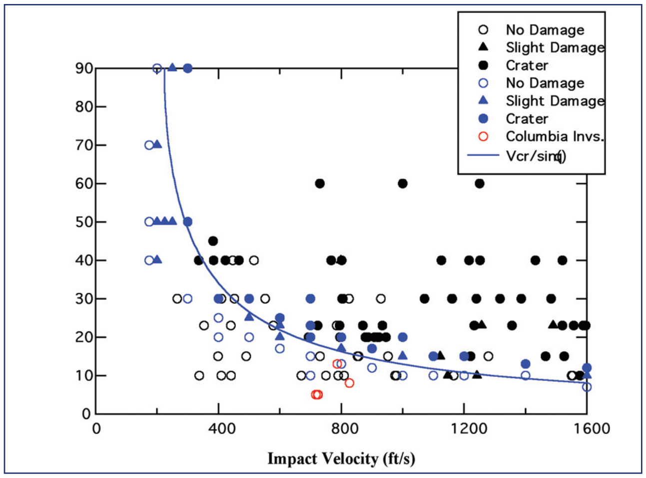

Figure 16. Theoretical damage/no damage transition curve with results of computations (blue) and all impacts into thermal tiles contained in [1,3] (black) and the Columbia investigation tests (red).

Impact into Tiled Surface of Orbiter

So far, the discussion has focused on the impact of a single tile by a piece of foam. From a theoretical viewpoint, the tile and foam can be of arbitrary size, so if a tiled surface behaved like a "large" tile, the above damage/no damage transition curve would carry over to the tiled surface of the Orbiter.

There are three differences between the tiled surface and a "large" tile:

1) On the Orbiter the tiles are attached to an aluminum substructure through a strain isolation pad. Both the pad and aluminum substructure introduce less stiffness to the problem, making it easier for the tiles to move. Per se, that is not a difference. The difference arises when the aluminum substructure stops moving. Then, due to the load being produced by the impacting tile, the aluminum structure flexes and, in some areas, increases the angle of incidence and thus increases the normal component of the velocity, thus increasing the stress on the surface. Thus, surface motion can lead to higher stresses which may crush the tile. In practice, it is unlikely the structure will flex very much, and so this is not a great concern.
2) The aluminum substructure could fail due to the load. This would not be a failure of the thermal protection system. As such, it is not considered here.
3) In the Orbiter configuration, the tiles are separated and a gap-filler is placed between the tiles. On impact with foam, the edges of the tiles are essentially being struck at a much higher incident angle and are therefore undergoing larger stresses than the flat top of the tile. Crush-up of the tile could begin at the edges and then propagate across the tile surface causing more damage.

In practice, for foam insulation impacts on tile, only "3" is a concern.

The testing performed by NAIT/CAIB during the Columbia investigation included the impact of a main landing gear door from Enterprise to which thermal tiles had been added. Five tests were performed (Table 6). All these tests were with velocities and angles that were well below the damage/no damage transition curve. The critical angle is the angle obtained from Eq. (10) for the given impact velocity and V_{crush} = 68.2 m/s. Thus, no crush-up of the tile is to be expected, and none was observed. There was minor damage done to the tiles, but all of it appeared to be due to edge damage due to the foam hitting or catching on an edge of the tile. Thus, the impact testing for the Columbia investigation agrees with the theoretical damage/no damage transition curve presented here.

Effect of Changes in Material Properties

One of the benefits of a good theoretical model is that it is possible to explore the role of material properties. For example, material properties could lie outside the expected ranges, and it is desirable to know how such variation affects the results.

In this vein, two variables were considered. First, the question of what would be the effect of doubling the foam density is addressed. If the foam density is doubled from the value of 2.4 lb/ft^3 (0.03844 g/cm^3) to 4.8 lb/ft^3 (0.07688 g/cm^3), Eq. (8) gives that the new crush-up velocity is V_{crush} = 49.7 m/s (163 ft/s), or a reduction of 27%. When plotted on the previous graph, the result of such an increase in density is clear: it reduces the allowable angle for a given speed by about 25% for speeds above 400 ft/s (Figure 17).

In a similar fashion, the question of what would occur if the thermal tile crush-up strength was reduced by 20%, from 345 kPa (50 psi) to 275 kPa (40 psi), was considered. Such a reduction has a much more severe effect on the damage/no damage transition curve: V_{crush} = 39.2 m/s (129 ft/s), and the allowable angle is reduced about 40% for a given impact ve-

Impact Speed (ft/s)	Impact Angle	Critical Angle	Damage
723	5°	18.0°	Small gouges initiating at edges
717	5°	18.2°	None
725	5°	18.0°	None
827	8°	15.7°	Small gouges initiating at edges
787	13°	16.5°	Small gouges initiating at edges

Table 6. Test Summary from Main Landing Gear Door Impact Tests.

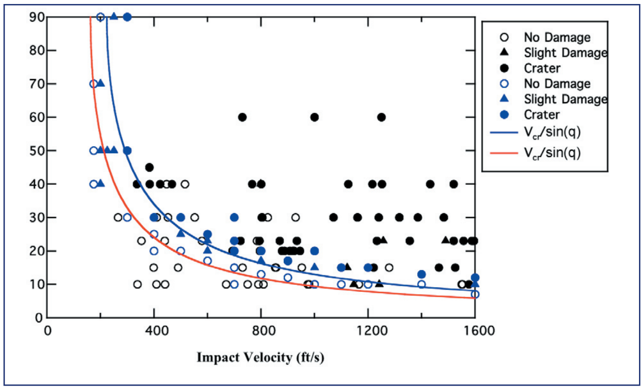

Figure 17. Effect of doubling the foam insulation density on the damage/no damage transition curve (red).

locity for velocities above 400 ft/s. Thus, tile failure is more sensitive to tile crush-up strength than relatively large variations in foam density. The condition of the tile is therefore of more concern than variations in foam properties.

Effect of Rotation of the Foam Impactor

The video footage of the foam insulation debris traversing the path from the external tank to the Orbiter wing shows a flickering that is likely due to rapid rotation of the foam insulation debris. Initial estimates put the rotation rate at 30 Hz, though by the time the RCC panel impact work was performed the rotation rate estimate had been lowered to 18 Hz. Since it is difficult to have controlled rotation during a ballistic test, the effect of rotation was examined computationally and then an equivalent non-rotating-impactor impact scenario was determined. The equivalent scenario involved an impactor of smaller size but a greater impact angle.

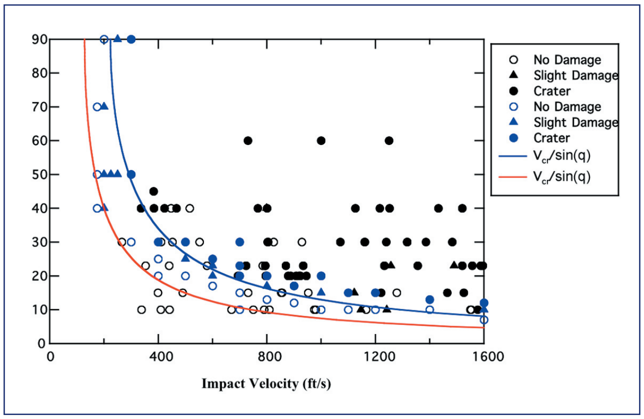

Figure 18. Effect of reducing tile strength 20% (red).

At first it may seem that rotation could not affect the impact a great deal. However, since it is normal velocities that matter, the rotational velocity can have a large effect. The maximum velocity due to rotation is given by the distance from the center of the rotation times the angular velocity:

$$v = \omega r \qquad (11)$$

For a piece of foam 19” long rotating at 30Hz about its center, the tangential velocity at the outer edge is 150 ft/s (45 m/s). Thus, since the crush velocity is 224 ft/s (68.2 m/s), it is clear that if the rotating foam impacts the surface in such a way that the rotational velocity is normal to the surface, then the rotational velocity can provide a significant percentage of the velocity required to reach the crush-up threshold.

The particular case of a 775 ft/s impact at 8° impact angle was considered. The theoretical damage/no damage transition curve above (Eq. 10) gives a critical angle of 16.8°, and therefore, no damage would be expected from the impact. In this case the impactor has assumed dimensions of 19” × 11.5” × 5.5” (though the latter dimension will not enter in, as the computations will be 2D plane strain). The normal component of velocity is 108 ft/s. The 30 Hz rotation rate at 9.5” gives a speed of 150 ft/s. Thus, the sum of these speeds exceeds the 224 ft/s crush-up velocity. That means that given the right orientation at impact, the rotation of the foam impactor can change what would otherwise be a non-damaging impact against the thermal tile to a damaging one.

Computations were performed for the above impact geometry for a counterclockwise rotation, no rotation, and a clockwise rotation. Lacking a full model for a tiled surface, a single “large” tile was used to represent the thermal tile. Figure 19 shows the results of the CTH computations for the three cases. The figure shows the σ_{yy} stress. The images in the left column are for the impactor rotating counterclockwise, the center column is the non-rotating case, and the right column is the clockwise rotation. As time progresses (0, 1, 2 and 5 ms) it can be seen that the counterclockwise rotation prevents an impact on the front end of the impactor, and rather for this case the back end impacts first. For the counterclockwise case, little damage is done to the tile. As predicted, there is no crater formed for the non-rotating case. For the clockwise rotation case, however, the leading edge impacts with a normal velocity above the crush-up velocity and a crater is formed in the tile. Thus, for the clockwise case, rotation leads to damage of the thermal tile. Figure 20 shows the normal stresses at the tracer locations for the three cases; these normal stresses confirm the damage seen from the previous figure, namely that the stresses are below the 345 kPa (50 psi) tile crush stress for the counterclockwise and non-rotating cases and are well above the tile crush stress for the clockwise rotation case.

Computations were then performed to determine an equivalent non-rotating impactor to mimic the clockwise rotating case. It was assumed that the impact velocity would be the same – 775 ft/s. As a first step, it is clear that to achieve the same result seen in the clockwise rotating case it is necessary to exceed the critical angle of 16.8° degrees, because unless that angle is exceeded, no damage will occur in the tile. Thus, computations were performed at impact angles of 17° and 18°. In order to obtain a loading time similar to that produced by the rotating impactor, it was necessary to reduce the length of the foam impactor. A similar loading time is necessary because the loading time determines the depth and extent of the crater; using the same size impactor results in too long and too deep a crater. An impactor length that produced a similar crater in the tile was 9.5” (half the original length). Figure 21

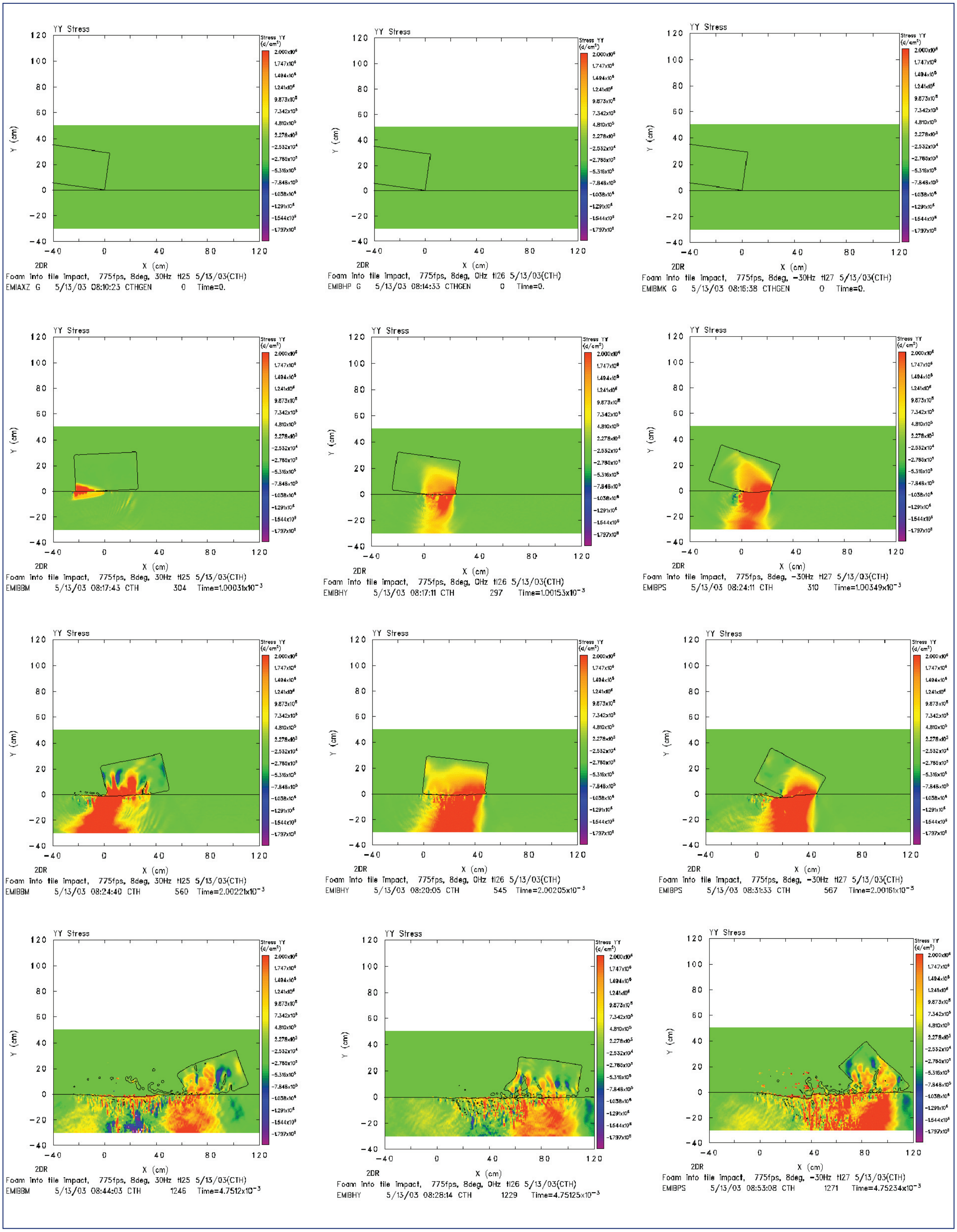

Figure 19. Comparison of rotation cases for 775 ft/s impact at 8° angle, 30 Hz counterclockwise in left column, no rotation in center column, 30 Hz clockwise rotation in right column. Times are 0, 1, 2 and 5 ms.

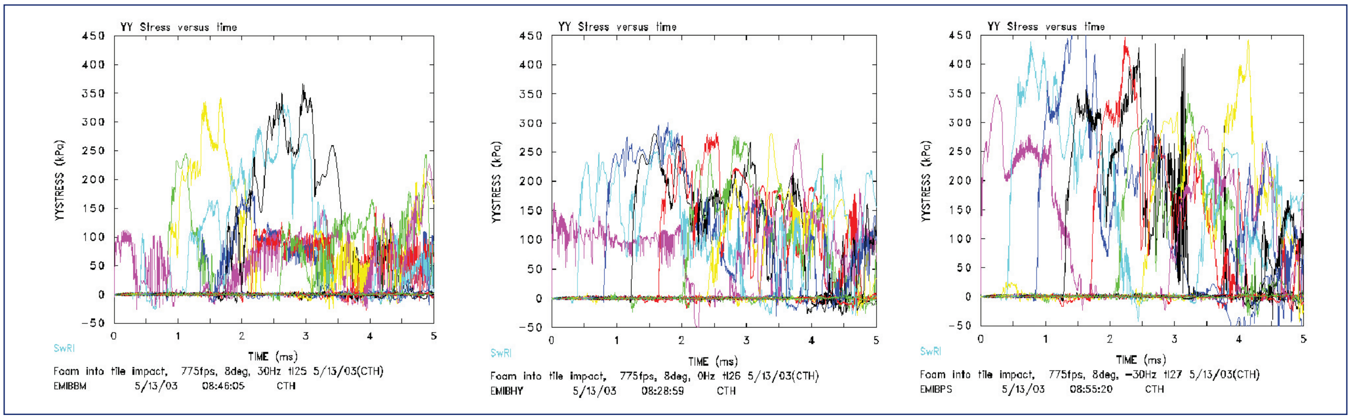

Figure 20. Normal stresses from rotation case comparison, left is 30 Hz counterclockwise, center is no rotation, right is 30 Hz clockwise. For the clockwise case, the stresses clearly exceed the 345 kPa (50 psi) crush-up stress of the tile, and damage is expected.

shows the σ_{yy} stress from three impact cases: 8° with 30 Hz clockwise rotation with the original sized impactor (left column), and 17° (center column) and 18° (right column) non-rotating impactors of half the length, or dimensions of 9.5” × 11.5” × 5.5” (though again the last dimension doesn’t enter in as the computation is 2D plane strain). It can be seen that all three impacts are producing similar stresses and craters in the tile. Figure 22 shows the normal stresses at the tracer locations. The tracers for the three cases are similar. Thus, to replicate the influence of 30 Hz clockwise rotation rate of the 8°-impact-angle impact one would use a non-rotating half-length projectile at a considerably higher impact angle of 17° or 18°. This equivalent impactor is determined based on how the tile crushes up and, in particular, that damage depends on the load delivered at the surface.

Though it is not considered here, another way to obtain similar damage would be increase the velocity of the foam impactor, rather than the impact angle, since increasing the impact speed while keeping the impact angle the same also increases the normal velocity. Using Eq. (10), if the impact angle of 8° were to be kept the same, then the impact velocity would need to be increased to at least 1610 ft/s (491 m/s) to begin damaging the tile. Calculations would need to be performed at these higher velocities to determine the new size of the impactor to produce similar damage. The approach is the same as that done above for the equivalent impactor at the higher impact angle.

RCC Impact Modeling

During the course of the investigation, attention moved away from the thermal tiles towards the leading edge. The leading edges are made of panels of reinforced carbon carbon (RCC).

Modeling of the impacts of RCC Panels performed during this investigation involved two major assumptions:

1) The RCC material was modeled as an isotropic elastic solid;
2) The foam impact on the outer face of the RCC Panel was handled through an analytic boundary condition.

These assumptions will be discussed below. A consequence of assumption #1 is that there is no damage model and thus no failure: stresses in various parts of the panel assembly were computed and conclusions about damage to panels will be based on the two experiments performed. In general, though, the stress levels are used to compare the results of various parameter studies for the impact event. Assumption #2 will be discussed in detail below; one of its consequences is that load calculations are an upper bound to the loads that would be delivered by the foam impactor to the panel.

Due to lack of detailed damage information as well as material properties, it was decided to model the RCC material as a purely isotropic elastic solid and to examine the history of the stress in various regions of the RCC panels during impact to study the impact event. The properties from the Rockwell International Materials and Processes Report “Shuttle Orbiter Leading Edge RCC T-Seal Cracking Investigation” (M. R. Leifeste, A. R. Murphy and S. V. Christensen, LTR 4088-2401, November 1991) give Young’s moduli of 4 to 10 Msi. Experimental work performed by Sandia National Laboratories Livermore as part of the Columbia investigation (W-Y Lu, B. Antoun, J. Korellis and S. Scheffel) gave Young’s moduli of 0.6 to 2.5 Msi. (Part of the reason for ranges in value is due to tests in different orientations and differences in tension and compression results.) For the computations performed here, the value of 20 GPa (2.90 Msi) was used. The density was taken to be 1.6 g/cm^3 and the Poisson’s ratio was taken to be 0.27. These three values completely specify the behavior of RCC material in the modeling. Within the code other values were computed from these values for use, such as the bulk modulus $K = 14.5$ GPa, the bulk wave speed $\sqrt{(K/\rho)}$ = 3009 m/s and the shear modulus 7.87 GPa. The material properties for the RCC are summarized in Table 7.

ρ	*E*	*Poisson’s Ratio*
1.6 g/cm^3 *100 lb/ft^3*	*20 GPa* *2.9 Msi*	*0.27*

Table 7. RCC Material Properties Used in the Modeling.

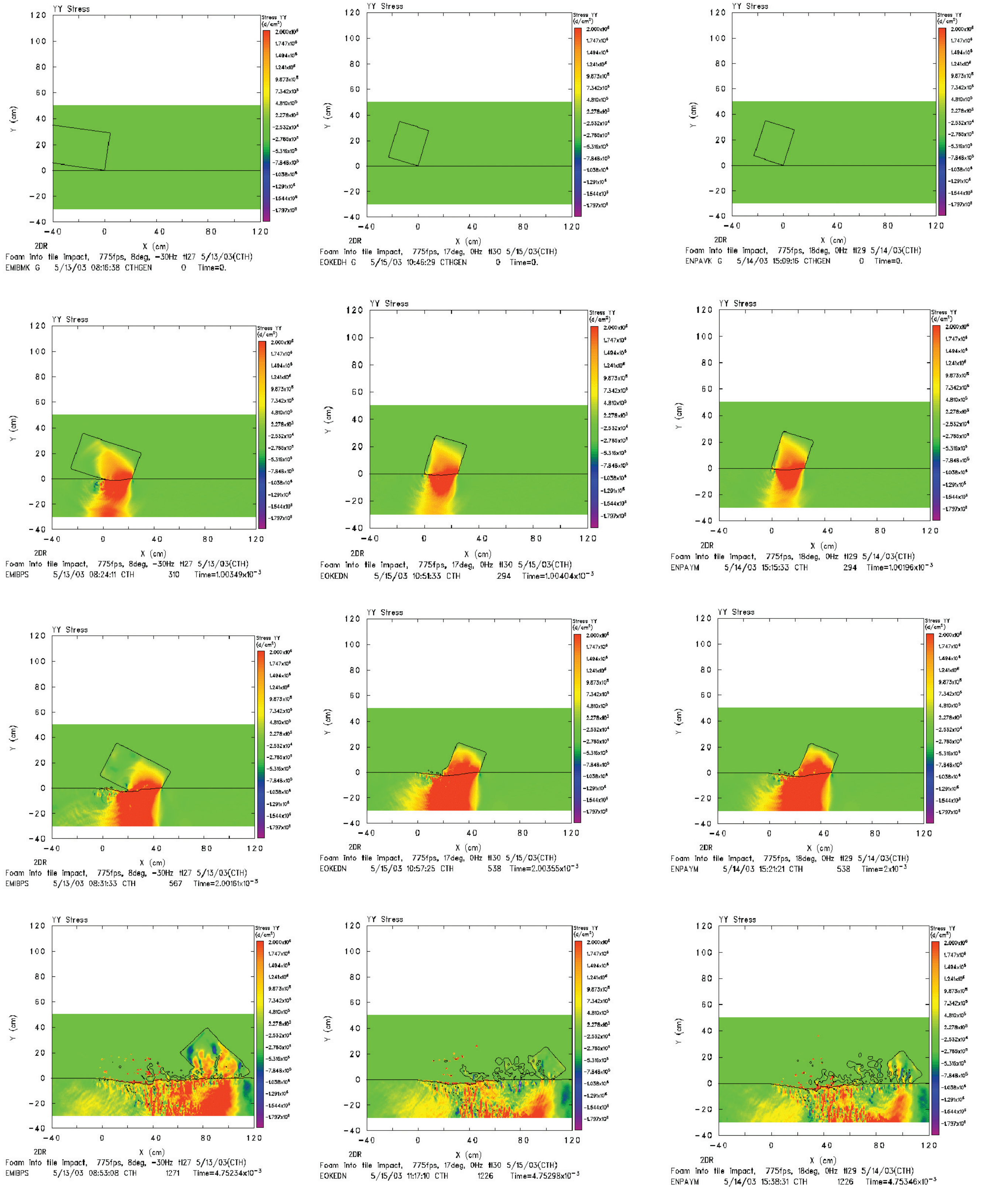

Figure 21. Nonrotating impactor to produce similar damage as 30 Hz clockwise rotating impactor. 30 Hz clockwise rotating impactor at 8° angle in left column, 17° degree nonrotating impactor in center column and 18° nonrotating impactor in right column. All impacts at 775 ft/s. Figures show σ_{yy} stress. Times are 0, 1, 2 and 5 ms.

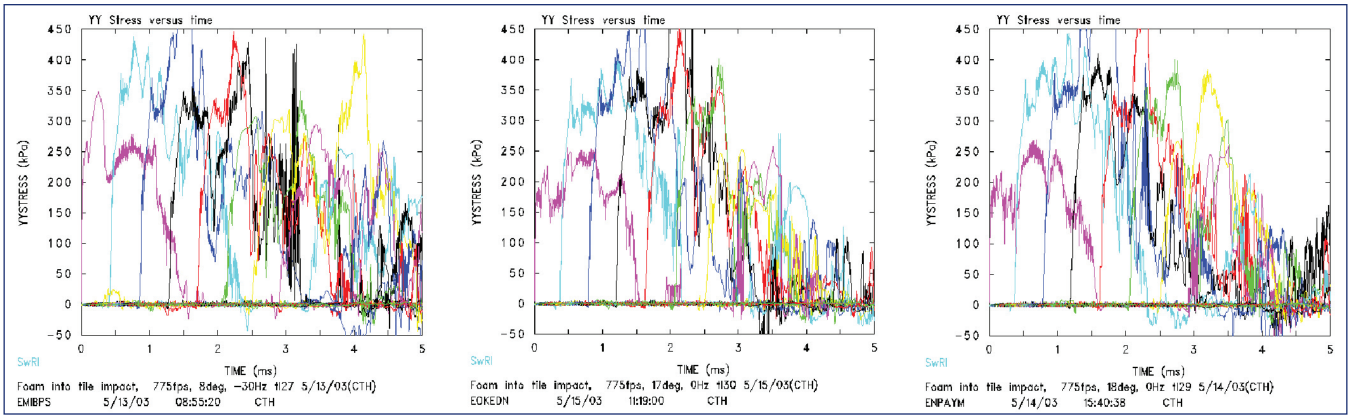

Figure 22. Nonrotating impactor to produce similar damage as 30 Hz clockwise rotating impactor. 30 Hz clockwise rotating impactor at 8° angle in left column, 17° degree nonrotating impactor in center column and 18° nonrotating impactor in right column. All impacts at 775 ft/s. Graphs show normal stress at tracer locations versus time.

Early attempts to model the problem with CTH, as done above for the tile impact, were unsuccessful. In the past, SwRI has had difficulty modeling thin plates with CTH, as the tensile states lead to void insertion and failure of the plates. Attempts to perform impact calculations against thin plates, even with 10 cells across the thickness of the plate, were unsuccessful, and so it was decided to pursue a Lagrangian model of the RCC panel.

To model the RCC panel in the Lagrangian frame, new software was written. The coding was based on the finite difference/finite volume algorithms used in HEMP 3D and detailed in [4]. The mathematics of these algorithms is similar to that of explicit finite element codes (for example, DYNA) and it allows for large deformation and large deflection. The written software's implementation was verified by computations involving wave propagation at arbitrary angles and plate vibration at arbitrary angles. The solutions from the new code produced the correct wave propagation speeds and magnitudes and the correct vibrational frequencies. Performing the test cases at arbitrary angles with respect to the coordinate system ensured that the whole stress tensor was being engaged and that the implementation was correct, hence verified.

To simplify and speed up the computations, it was decided to handle the foam insulation impact through an analytic boundary condition based upon the results of the work detailed above. The stress at the boundary was written as a function of the foam velocity, the local material velocity, and the angle of impact. In particular,

$$p = \begin{cases} \rho_{0f} c_{0f} (V - u_{RCC}) & V \le u_{RCC} + u_{ef} \\ \sigma_{crush\text{-}f} + \rho_{ef} (c_{1f} - u_{ef})(V - u_{ef} - u_{RCC}) & V > u_{RCC} + u_{ef} \end{cases} \qquad (12)$$

where V is the velocity of the foam normal to the surface and u_{RCC} is the velocity of the RCC material normal to the surface. Thus, an explicit analytic expression for the pressure has been obtained from Hugoniot jump condition considerations outlined above, and shown to agree with the CTH computations performed during the tile impact study. Figure 23 shows the dependence of loading pressure on velocity (in particular, on $V\text{-}u_{RCC}$). The impacts during the testing program were at 775 ft/s with the local impact angles typically between 10° and 25°, the angle varying since the leading edge panels have curvature. Thus, the normal velocities were between 135 and 330 ft/s, with pressures between 40 and 65 psi. These values give some idea of the expected loads. Two impacts of foam insulations against RCC were performed. The modeling will be discussed below, but for now the footprints of the impacts are shown in Figure 24. For the RCC Panel #6 impact (to the left), the maximum loading footprint has an area of 110 in^2 (712 cm^2) roughly corresponding to a triangle of base 20" and height 11". If the panel doesn't move, there is an average pressure of 55.6 psi (384 kPa) for a 768 ft/s impact at the appropriate impact orientation. Thus, the expected maximum load is 6140 lb (2.73×10^9 dynes). (The actual load during the impact will be less due to panel material motion since $u_{RCC} > 0$.) The area-averaged impact angle is 19.7° (that is, this angle is the average interaction angle based on the foam impactor's velocity vector and the surface normals of the surface cells). For the RCC Panel #8 impact (to the right), the quadrilateral footprint has an area of 193 in^2 (1246 cm^2) and is roughly 17" across and 11.5" high. If there is no panel motion the average pressure would be 52.9 psi (364 kPa) for a maximum load of 10,200 lb (4.55×10^9 dynes). The area-averaged impact angle is 17.5°. In both cases the foam impactor delivers a substantial load to the panels. Errors from the analytic load approximation are reduced by the fact that the loading occurs in the region of the pressure-velocity curve with the shallower slope: thus, when rarefactions tend to reduce the loading pressure, the change in pressure is less than if the loading response of the foam were such that it did not have the relatively level stress portion after the crush-up point is reached (Figs. 23 and 24). In any event, loads computed from the analytic expression (Eq. 12) are upper bounds for those that would be observed in an actual impact event.

Based on the properties of the RCC used in this analysis, the longitudinal wave speed in the RCC material is 3950 m/s, and so the particle velocity in the RCC at the foam's crush stress is 3.5 cm/s. Thus, relative to the foam, the RCC material is a rigid surface. Thus, the material velocity of the RCC material due to elastic waves in a thick material resulting the impact with the foam is not large, and is in fact negligible compared to the structure motion of the plate. However, as will be seen, the velocities associated with the structural motion of the plate are large enough that they must be included. The u_{RCC} term in the above equation includes all motion of the RCC panel, including small elastic motions due to elastic wave transit and the larger structure motions that the panel undergoes during the impact event.

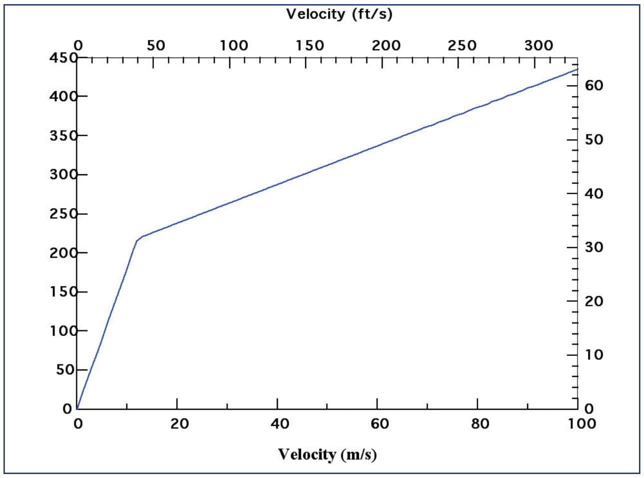

Figure 23. Pressure vs. velocity for the analytic boundary condition.

The only failing of the analytical pressure boundary condition as presented in Eq. (12) is that it does not include the reduction in pressure that can occur from relief waves returning from the free surfaces of the foam (note that the waves propagating outward from the impact point are correctly included, as is the material motion of the RCC panel material and the free surface on the interior of the panel) and the reduction in pressure that can occur from the fracture of the foam impactor. Due to not including these relief waves, the computed load will be greater than the actual load and can be viewed as an upper bound. Though there is some unloading from the elastic wave, unloading that causes the foam impactor to lift away from the panel face is controlled by the wave speed c_{1f} = 49.8 m/s. Thus, with the thickness of the foam impactor being 5.6”, and assuming a compressive strain of 50% (so that the total travel distance for the wave is 5.6”), the time of unloading is on the order of 2.9 ms.

CTH computations with this impactor also showed that the loading for impact velocities on the order of 775 ft/s and angles of on the order of 20° and less produced unloading times on the order of 2 ms and greater. The time it takes to travel 20”, roughly the furthest distance along the panel face the impactor travels (see Figure 24), is 2.3 ms. Thus, the geometry and impact conditions are fortuitous in that for the foam impactor considered here (with a thickness of 5.6”) and with the impact angles and velocities considered here (leading to a 20” long or less loading path), the unloading from the free surface of the foam impactor occurs as the foam impactor is extending beyond the panel face. Thus, the unloading behavior does not need to be included in the boundary condition for these computations. As will be seen, the maximum load is typically achieved by 2 ms during the foam impacts on the RCC panels. Breakup of the foam insulation impactor can occur due to the way the impactor flexes when striking the curved panel surface or by catching on a sharp edge; in the tests, impactor breakup was observed later in the impact event (later than 2 ms) either due to impacting the T-seal, twisting of the foam impactor, or impact with the sharp edge of a hole. Thus, the lack of including unloading effects due to relief waves and fracture in the foam is not detrimental. (The lower corner of the foam impactor can be seen to leave the panel face in the test against RCC Panel #8, but this departure is as the foam is leaving the panel face and does not greatly affect the load).

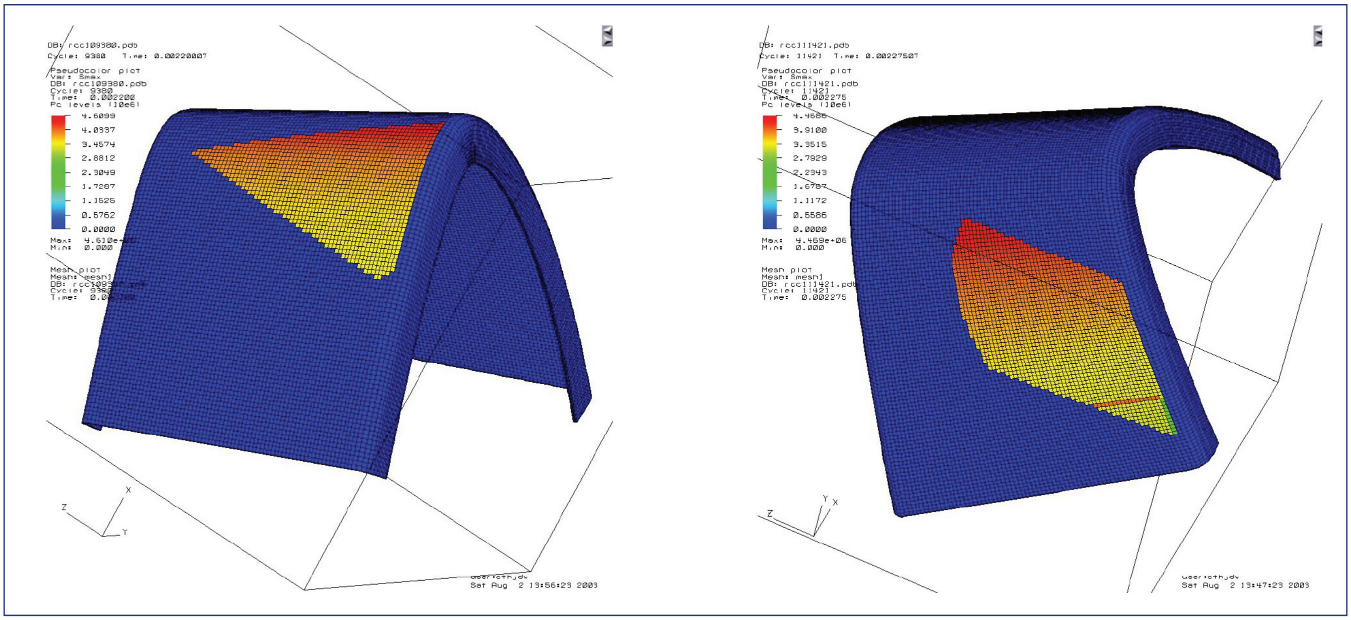

Figure 24. Footprints of impacts against RCC Panel #6 (left) and RCC Panel #8 (right).

Two panels were modeled, Panel #6 and Panel #8. Both were modeled in a similar fashion. The zoning was 4 zones through the thickness of the panel, 100 zones from side to side, including ribs, and 200 zones from bottom to top. In addition, the bottom flange was modeled for both, with 4 zones through the flange and the appropriate connections with the panel. For the connection of the panel with the ribs, a smooth transition from panel to rib was made with a radius of curvature of 0.8" for Panel #6 and 1.0" for Panel #8.

As to geometric details of the two panels, both were constructed taking two curves from the Pro-E model delivered to SwRI by Jim Hyde in May, 2003. The coordinate system in the file is what was used in the computations, which the author is told are in the "Wing Coordinate" system. The curves defined the inboard and outboard edges of the panel geometry. Measurements were then taken from the panels when they were on hand at SwRI to determine the various thicknesses, and these thicknesses were then used in the model. In particular, the thickness of the panel, ribs, and flange for Panel #6 was 6.7 mm, as measured from RCC Panel #6. This value compares to the stated value of 0.233" (5.9 mm) according to Boeing supplied information. For RCC Panel #8, the thickness of the principal part of the panel was again 6.7 mm, with the ribs after the curve 9.5 mm and the flange 8.0 mm. Also, for the lower portion of Panel #8 there is a doubler that increased the thickness of panel on the lower panel face from 6.7 mm to 8.0 mm. Again, these values are based upon measurements taken from RCC Panel #8 while at SwRI.

To approximate the boundary conditions, the bottom of the rib on both the upwind side and the downwind side and above the wing and below the wing were pinned so that they could not move.

Diagnostics taken from each computation were the maximum principal stress in the panel face, the maximum principal stress in the rib, the total load, and the maximum displacement anywhere on the whole panel and the maximum velocity anywhere on the panel (though these tended to be near the center of loading on the panel face). All the stresses through the thickness of the panel were included; for example, the maximum principal stress on the panel face was typically on the back face (wing interior) of the panel. In computing the maximum principal stress for the panel face, the region considered did not include the flange connection, as large stresses sometimes arose there due to boundary condition behavior that is not representative of the panel face. Also, the maximum principal stress in the rib was measured away from the pinned ends, since large stresses arose at the connections that are not representative of the actual boundary conditions at the rib. The actual boundary condition in the test fixture and on the Orbiter has more slop.

The reference frame of the panel was taken to be the same as that supplied in the initial Pro-E file. Thus, the angles discussed below should be the same as those used during the testing program. The z-axis goes from the front to back of the Orbiter, the y-axis from the bottom to top of the Orbiter, and the x-axis is perpendicular to the y- and z-axes and runs in the lateral direction. The direction of travel of the foam impactor when it impacts the RCC panel is determined by the angles α and β: α is the angle between the z-axis and the foam impactor velocity vector in the y-z plane (or the difference from a right angle between the velocity vector and the y-axis in the y-z plane) and β is the angle between the foam impactor velocity vector and the z-axis in the x-z plane (or the difference from a right angle between the velocity vector and the x-axis in the x-z plane). Thus, the direction $\alpha=0$, $\beta=0$ is the negative z-axis direction: that is, the foam impactor is traveling directly along the main Orbiter axis from the front of the vehicle to the back. β positive means the velocity vector is pointing away from the center of the vehicle and α positive means the velocity vector is pointing from the bottom to the top of the vehicle (these qualitative statements are for small angles). Thus, positive α means that the foam impactor is hitting the underside of the leading edge at a steeper angle, and positive β means that the foam is traveling away from the centerline of the Orbiter when it impacts the leading edge. Increasing α increases the impact angle. Unfortunately, the angle β's influence is more complicated and ties into the impact geometry, the shape and orientation of the foam, where the foam impacts with regard to the curved leading edge and the path the foam takes (needed for computing an "average" impact angle). In general, increasing β tends to increase (in an integrated average sense) the impact angle.

Overview of RCC Panel Impact Computations

Results of twenty-one computations of impacts of foam against RCC panels will be presented. For discussion purposes, it seems that presenting the modeling of the two tests allows the best explanation of the results of the computations and their interpretation. After the comparisons with the two test cases are presented, calculations will be described that examined the role of impact location, impactor rotational velocity, and impact angle.

Impact on Panel #6 for Test Impact Condition

During the testing program, one impact was performed on RCC Panel #6. The impact conditions were a foam impactor of dimensions 21.4" × 11.6" × 5.6" (all impact computations into RCC panels in this report have these dimensions), flying at 768 ft/s and impacting at an angle of $\alpha=5.5°$, $\beta=2.5°$. The impact location was 18.7" from the bottom of the panel at the carrier panel interface and 0.83" aft of the 5-6 T-seal. These impact conditions were replicated in a computation in the model that was run to 5 ms after impact.

Figure 25 shows some stills from the computation. In the figure, the outline of the foam impactor as if it did not deform is shown (though the boundary pressures are provided analytically, as described above). All figures of the panel computations were made with Lawrence Livermore National Laboratory's MeshTV software. The panel is shaded to show the maximum principal stress at the given surface – that is, when looking on the outer panel face, the maximum principal stress in the outer layer of cells will be used, while looking at the inner surface of the panel face, the stresses from the innermost layer of cells will be used. The scale changes for each frame in the figure.

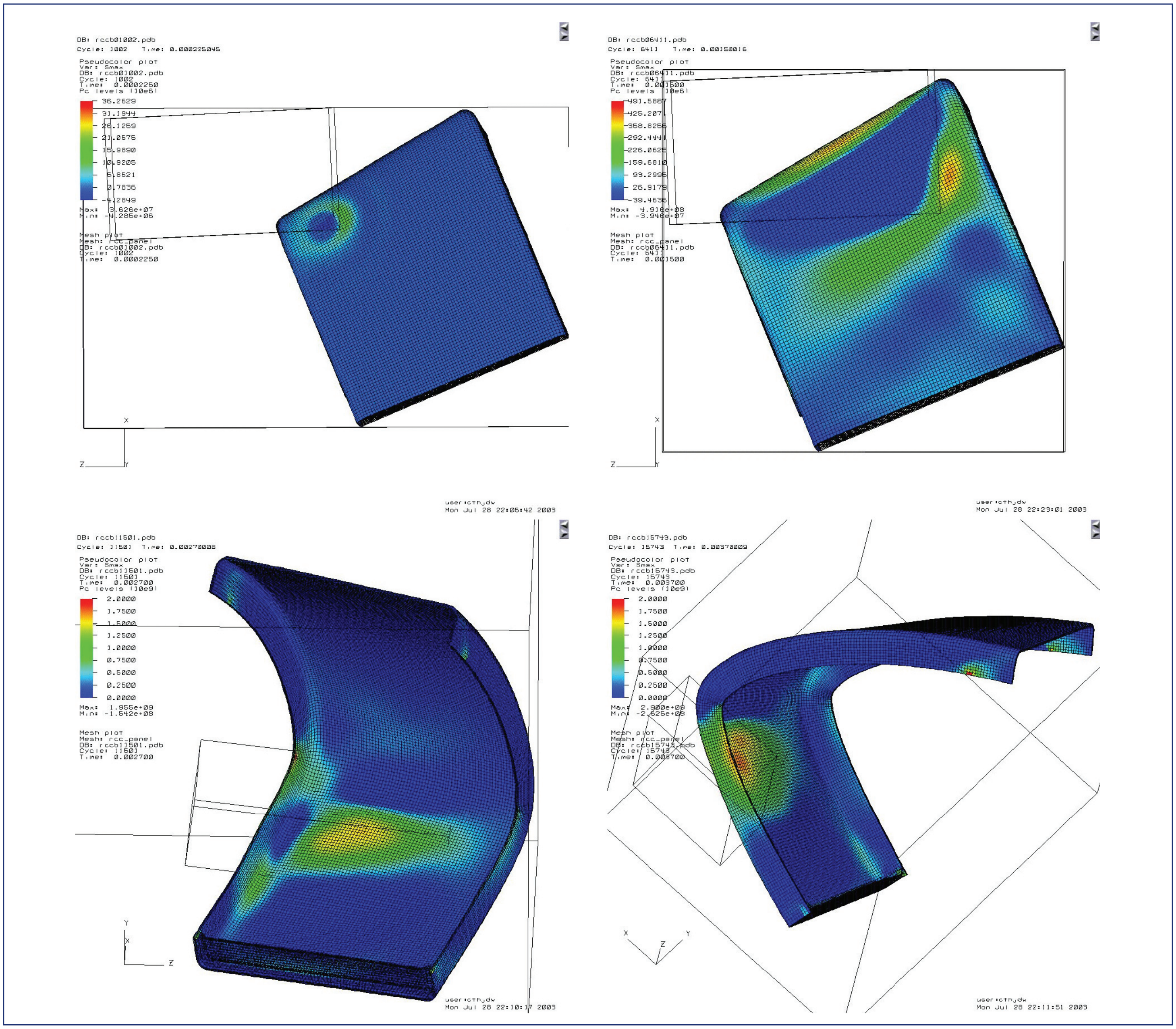

Figure 25. Four frames of the RCC Panel #6 test condition calculation (▯=5.5°, ▯=2.5°, 768 ft/s), at 0.225, 1.5, 2.7 and 3.7 ms. The 2.7 ms frame is where the peak rib stress is achieved near the greatest curvature of the rib; the 3.7 ms frame is where the outward flexing of the rib achieves the greatest stress.

RCC Panel #6 768 ft/s (234 m/s) α=5.5°, β=2.5° 18.7″ up from carrier panel 0.83″ from 5-6 T-seal 0° clocking angle	Load: 5850 lb (2.60×10^9 dynes) Panel stress: 26.8 ksi (185 MPa) Rib stress: 29.2 ksi (201 MPa) Displacement: 1.2 in (30 mm) Velocity: 102 ft/s (31.2 m/s)
RCC Panel #8 777 ft/s (237 m/s) α=5.5°, β=5.0° 25.5″ up from carrier panel 7.3″ from 7-8 T-seal 30° clocking angle	Load: 9150 lb (4.07×10^9 dynes) Panel stress: 43.2 ksi (298 MPa) Rib stress: 33.4 ksi (230 MPa) Displacement: 2.5 in (63 mm) Velocity: 137 ft/s (41.8 m/s)
(Option #3 – test condition)	

Table 8. Summary of Results of Test Conditions' Calculations.

Figure 26 shows the maximum principal stress seen in both the panel and the rib as a function of time as well as the load as a function of time. The left hand scale is in metric units for both the load and stresses. The right hand scale is in English units and applies to the stresses. The undulating behavior seen in the maximum principal stress curves is due to the fact that these curves are the maximum of many curves, one for each computational cell. Thus, as one maximum principal stress curve decreases, another increases and overtakes the original maximum principal stress cell, thus becoming the maximum principle stress cell itself. It can be seen that both the maximum principal stress in the rib and in the panel face are still increasing when the load decreases, thus showing that inertia plays an important role in the impact event. Finally, Figure 27 shows the maximum displacement and the maximum velocity seen on the panel during the impact event. Table 8 summarizes the historical maximums.

As was mentioned above, panel deformation affects panel loading. The panel is both deformed in shaped and is in motion, both aspects of which affect the local impact velocity, hence loading pressure, due to the foam impactor. The maximum average surface-normal component of the panel velocity over the loading area was 29 ft/s (8.9 m/s). This local velocity decreases the impact speed since the panel is being moved in the direction of travel of the foam impactor, thus decreasing the pressure load. However, the deformation of the panel led to an area-averaged angle of 20.1°, an increase over the 19.7° as would have been the case for the rigid panel. Because of the panel's deformed shape and higher angle than the rigid panel, the relative impact velocity increases (in average) to 264 ft/s (80.5 m/s) over the 259 ft/s (78.9 m/s) for the rigid panel, or an average increase of 5 ft/s. The deformed shape of the panel tends to increase the impact angle and thus increase the local pressure and the load delivered by the foam. However, since the area-averaged surface-normal velocity component at which the panel is moving away from the impactor is 29 ft/s, this overcomes the 5 ft/s increase in impact velocity due to increase in angle. Thus, overall, the load is less for the deforming panel than it would be for a rigid panel. On average, the pressure load (at maximum) for the deforming panel is 53.0 psi (366 kPa) while for the rigid panel it would have been 55.6 psi (384 kPa). This reduction is reflected in the maximum load in Table 8 versus the number given above for the rigid panel – a reduction of about 5%.

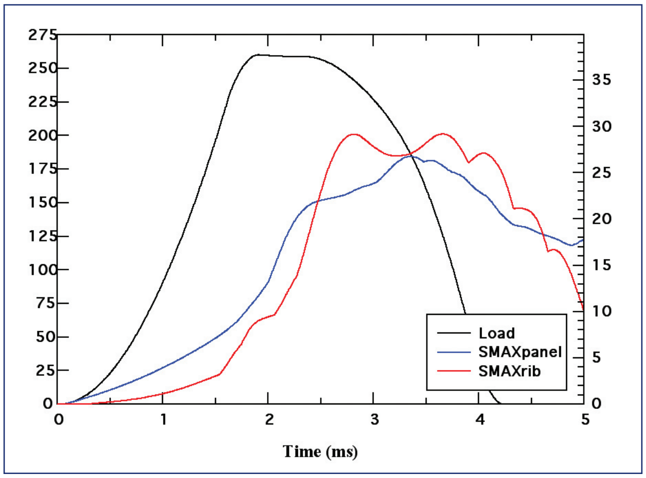

Figure 26. Load and maximum principal stress for panel face and rib vs. time for RCC Panel #6 test condition computation (α=5.5°, β=2.5°, 768 ft/s).

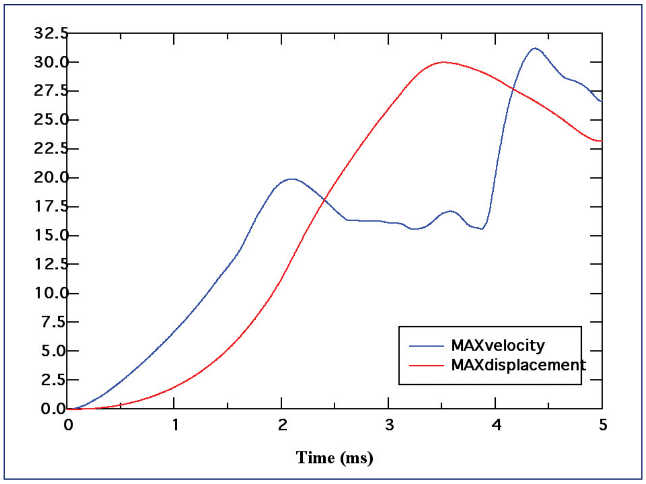

Figure 27. Maximum velocity and maximum displacement vs. time for RCC Panel #6 test condition computation (α=5.5°, β=2.5°, 768 ft/s).

As has been described, these computations are purely elastic, with no failure criteria. Thus, now it becomes necessary to interpret this computation in the context of the failure that occurred. Once failure occurs, the history of the stresses will change, and thus it is not possible to draw conclusions based on the behavior of the elastic calculations after the failure. As the RCC material is quite brittle, the use of the maximum principal tensile stress seems an appropriate failure measure.

In the test, the downwind rib broke, approximately 50 cm from the carrier panel. The crack ran, turning the corner slightly so that a small crack could be seen on the panel face.

If one reasons that a higher failure stress is expected in the panel (since there are no boundaries) than in the rib (since the rib has an edge where presumably there are many fracture initiation sites), then no rigorous information can be obtained from Figure 26. (If it were assumed that the maximum failure stress is the same in the panel face and the rib, then it could be concluded that the minimum maximum principal stress the RCC material can support is 21.9 ksi (151 MPa), the value of the maximum principal stress when the two curves of Figure 26 cross at 2.47 ms). However, we know that at some time the rib broke, and that this point was after some load had accrued. Looking at the curves, at early time the maximum principal stress in the panel is significantly above the maximum principal stress in the rib. Thus, it is likely that the failure occurred at a later time, probably in the vicinity of the larger stress observed, 2.7-3.7 ms. The mechanics of the larger stresses are as follows. As the foam impact loads the panels, a large tensile stress is created near the largest curvature of the outer edge of the rib (see Figure 25 at 2.7 ms). The location of this large maximum principal stress is approximately 55 cm from the carrier panel. The maximum principal stress in the rib is at this location from roughly 2.3 to 3.9 ms. Though the load reaches its maximum and then decreases, the stresses in the panel face and rib are still high or increasing. The loading becomes such that it causes an elastic buckling motion of the rib, so that the downwind rib (the rib next to the 6-7 T-seal) flexes outward (downwind). The flexing motion leads to large tensile stresses on the outside of the rib (Figure 25 at 3.7 ms), and for the period of 3.9 to 4.3 ms these are the large tensile stresses in the rib. The maximum value of the stress occurs about 42 cm from the carrier panel. As the load continues to drop while the foam impactor leaves the panel face, the buckling motion ceases, the rib straightens out and the region of the maximum tensile stresses return to the area near the largest curvature of the rib.

The interpretation now focuses on the time in this loading history that the rib broke. It is likely that it happened later in the loading process, perhaps at 3.7 ms, since the crack does not propagate very far in the face of the panel. The lack of crack propagation in the face of the panel implies that the load to the panel was decreasing when the fracture occurred. This reasoning implies that the rib fails at a maximum principal stress in the vicinity of 29 ksi (200 MPa), perhaps after some loading time (some damage theories hold that a tensile stress state must exceed a given value for a given length of time before failure occurs). This reasoning also implies that the panel face can support a 27 ksi (185 MPa) maximum principal stress.

Impact on Panel #8 for Test Impact Condition

A computation was performed for the impact test conditions on the Panel #8 impact, where the angles were α=5.5°, β=5.0°, with an impact speed of 777 ft/s (237 m/s). The geometry of Panel #8 is more complicated, as there are various thicknesses of RCC in the panel as described above.

In the test, the panel face failed, and a large hole was produced. An additional conclusion from the test is that it is likely the failure occurred at 2.7 ms or later due to the fact that half the foam impactor survived the impact. In the fiberglass tests and the RCC Panel #6 test, the foam impactor completely disintegrated, apparently due to the foam catching on the 6-7 T-seal. In the RCC Panel #8 test, the foam impactor is lifting off the panel (ricocheting due to the arrival of rarefaction waves) just before the 8-9 T-seal, but when the panel breaks the foam catches on the hole edge that is formed. Thus, examining the time sequence of impact from the computation, it is conjectured that the failure probably occurred (assuming it started near the 8-9 T-seal or near the downwind rib) around 2.7 ms.

Figure 28 shows the maximum principal stress in the panel interior versus time, as well as the maximum stress observed in the thick portion of the rib (the dotted portion of the maximum principal stress for the rib includes only the thicker part of the rib). In this test, the thick portion of the rib did not fail, whereas the panel face did. At 2.7 ms, the maximum principal stress in the panel face was 30.0 ksi (207 MPa) and in the panel rib was 25.4 ksi (175 MPa). Based on the results of the RCC Panel #6 test, these seem to be reasonable stresses for the failure. Once a crack forms, it runs quickly leading to extensive failure. Such failure was seen in the panel face. With failure of the face occurring around 2.7 ms, the load being transferred to the rib would reduce, and the stresses in the rib would decrease. This last statement is qualitative: there are inertial effects still, and so the stress could increase for a while. To quantitatively examine the histories beyond failure requires a failure model.

As with the RCC Panel #6 test conditions computation, panel deformation affected panel loading. The maximum average surface-normal component of the panel velocity over the loading area was 74 ft/s (23 m/s). This local velocity decreases the impact speed since the panel is being moved in the direction of travel of the foam impactor, thus decreasing the pressure load. However, the deformation of the panel led to an area-averaged angle of 19.9°, an increase over the 17.5° as would have been the case for the rigid panel. Because of the panel's deformed shape and higher angle than the rigid panel, the relative impact velocity increases (in average) to 264 ft/s (80.5 m/s) over the 234 ft/s (71.2 m/s) for the rigid panel, or an average increase of 30 ft/s. Since the area-averaged surface-normal velocity component at which the panel is moving away from the impactor is 74 ft/s, this overcomes the 30 ft/s increase in impact velocity due to increase in angle. Thus, overall, the load for the deforming panel is less

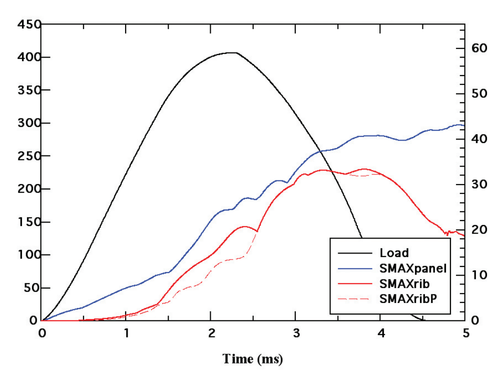

Figure 28. Load and maximum principal stress for panel face and rib vs. time for RCC Panel #8 test condition computation (α=5.5°, β=5.0°, 777 ft/s).

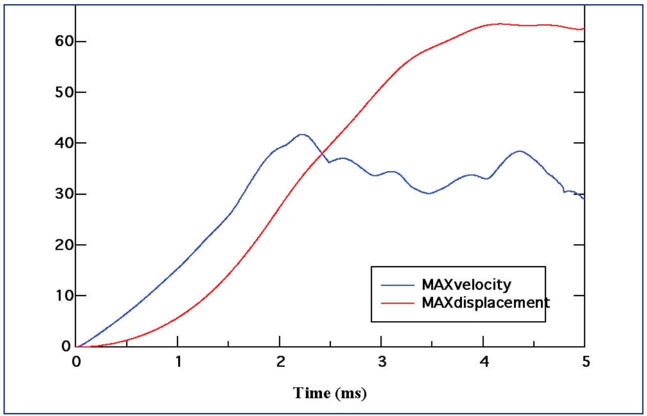

Figure 29. Maximum velocity and maximum displacement vs. time for RCC Panel #8 test condition computation (α=5.5°, β=5.0°, 777 ft/s).

than it would be for a rigid panel. On average, the pressure load (at maximum) for the deforming panel is 47.7 psi (329 kPa) while for the rigid panel it would have been 52.9 psi (365 kPa). (These pressures are lower than they were for the corresponding RCC Panel #6 test condition case above because the average impact angle is less.) This reduction is reflected in the maximum load in Table 8 versus the number given above for the rigid panel – a reduction of about 10%.

In summary, for the two impact tests performed, for the numerical model developed here, large cracks form in the vicinity of 28 to 30 ksi for the panel face and for the rib. These stresses correspond to roughly 1% strain in the material. These tensile stresses leading to cracks are viewed as being consistent within this model for analyzing the additional cases to be run. They are understood in the context of the two main assumptions made for this modeling: the isotropic elastic constitutive model and the analytic boundary condition, which is an upper bound.

Impact Location Study

One topic of interest was the effect of impact location on the load and stress seen by the panel. To explore this effect with the numerical model, a study of nine impact locations on RCC Panel #6 was performed with the impact velocity vector aligning itself with the Orbiter's z-axis (i.e., $\alpha=0°$, $\beta=0°$). The impact speed was 768 ft/s. The nine impact locations considered were variations of the impact location used in the RCC Panel #6 test with combinations of 3" and 6" down from the original impact point and 3" and 6" across from the original impact point.

Table 9 shows the maximum stresses seen in the panel interior and the rib for each impact case as well as the maximum load. The largest stresses are seen for the lowest and most upwind location on the panel. It can be seen that these values are large enough to assume the rib would fracture. It is interesting to note that the largest loads did not produce the

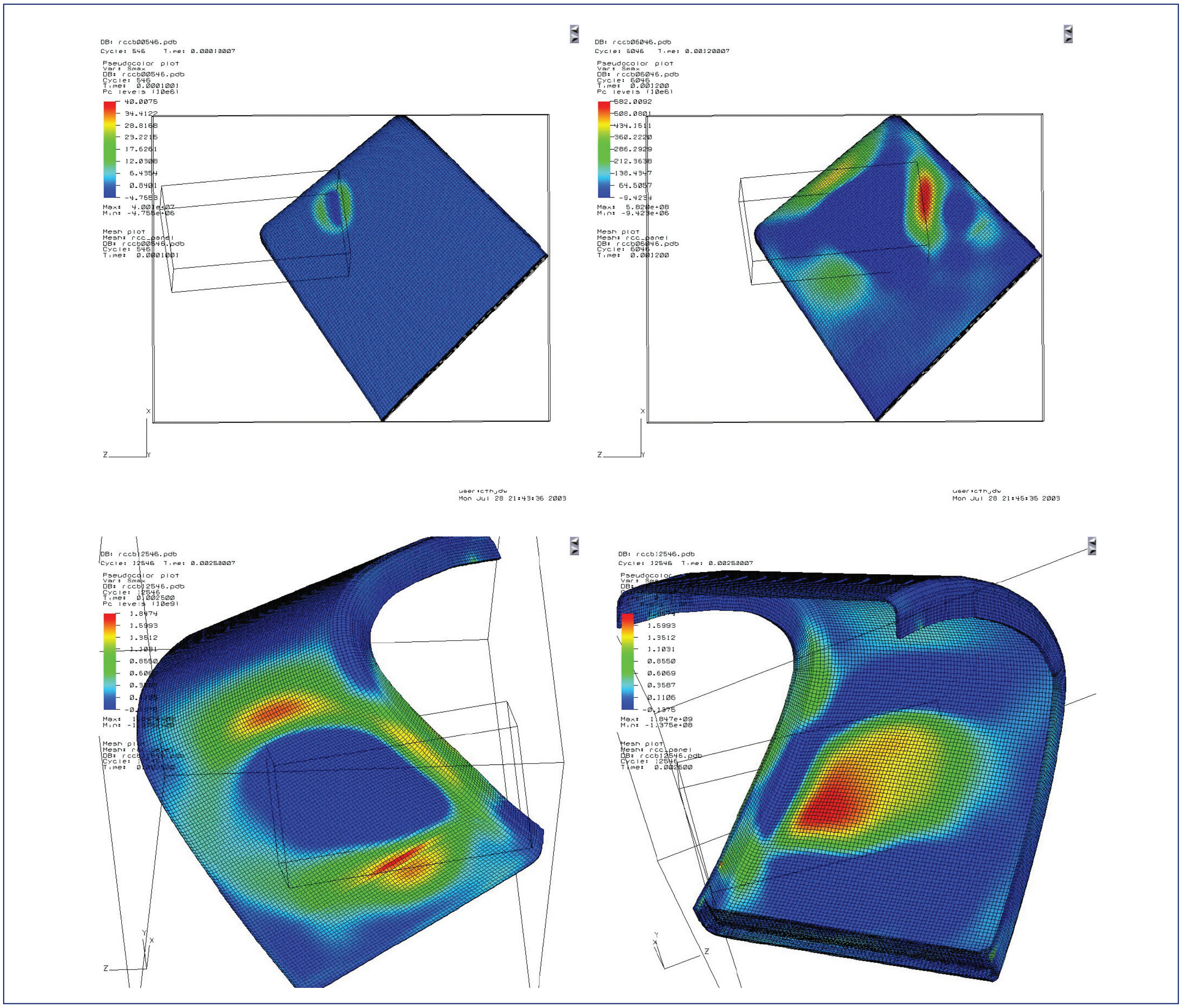

Figure 30. Four frames of the RCC Panel #8 test condition calculation (α=5.5°, β=5.0°, 777 ft/s), at 0.1, 1.2, 2.5 (front face) and 2.5 (back face) ms (the last two frames are probably near the failure time of the panel).

	0.83" from T-seal	*3.83" from T-seal*	*6.83" from T-seal*
18.7" from carrier panel	Load: 4680 lb Panel stress: 24.5 ksi Rib stress: 24.4 ksi	Load: 3330 lb Panel stress: 18.3 ksi Rib stress: 19.8 ksi	Load: 2150 lb Panel stress: 9.6 ksi Rib stress: 14.0 ksi
15.7" from carrier panel	Load: 4320 lb Panel stress: 25.8 ksi Rib stress: 27.5 ksi	Load: 3090 lb Panel stress: 21.9 ksi Rib stress: 20.6 ksi	Load: 2030 lb Panel stress: 15.5 ksi Rib stress: 13.6 ksi
12.7" from carrier panel	Load: 4290 lb Panel stress: 26.9 ksi Rib stress: 30.1 ksi	Load: 3040 lb Panel stress: 22.9 ksi Rib stress: 21.7 ksi	Load: 2000 lb Panel stress: 18.3 ksi Rib stress: 15.3 ksi

Table 9. Maximum Values for Load, Panel Stress and Rib Stress for Various Hit Locations (RCC Panel #6, α=0°, β=0°, 768 ft/s).

largest maximum principal stresses in the rib or panel face. This result is due to the fact that the largest loads occur when the foam impactor has the largest angle where it is impacting the panel. However, the large angle is on the curved portion of the panel, where the curvature of the panel allows the membrane stresses to support some of the load. (This support behavior is the cause of the surprising load supporting ability of shells, such as domes.) The higher loading pressures are occurring in a region of the panel where the geometry has curvature and is thus more able to support the load. As the impact point moves down the panel face into the flatter region of the panel, the loads decrease because the angle is decreasing and thus the loading pressure is decreasing. However, the ability of the panel to support the loads through curved (shell) geometry decreases as the flatter region of the panel is now being impacted, and the net result is larger stresses in both the panel face and the rib.

As a reference, results from the baseline impact (the same impact location as the RCC Panel #6 test but with α=0°, β=0°) are presented. Figure 31 shows stills of maximum principal stress at four times: 0.2, 1.2, 2.5 and 3.5 ms. Figure 32 shows the stress history of the panel, and Figure 33 the maximum velocity and displacement. The same three-hump behavior can be seen in the rib stress as was observed in the actual test condition calculation, due to loading near the maximum curvature and then a downwind buckling type flexure of the rib. As the impact continues, the load from the foam projectile decreases as the loading area decreases as the foam continues to travel, and the buckling motion is relieved, and the rib straightens out. This places high stresses at the top of the arch, which are the high stresses seen in the 4 to 4.5 ms time frame in the stress history plot. The stress upon release of the buckling is especially high for the maximum stress case (impact point at 0.83" from 5-6 T-seal, 12.7" up from carrier panel) and is shown in Figs. 34 and 35. Though the maximum stress in the rib is a little higher in the earlier impact times (2-4 ms), it is the large peak upon the straightening of the rib between 4 and 5 ms that puts the maximum principal stress over 30 ksi (207 MPa). The impact location with the most severe stresses increased the maximum panel face stress by 10% and the maximum rib stress by 23% over the baseline.

Similarly, two impact conditions for RCC Panel #8 were considered, referred to as "Option #3" and "Option #2" during the RCC Panel #8 test design. "Option #3" was chosen for the actual test that was performed. "Option #2" is essentially a 3" shift towards the 7-8 T-seal. Based on the results outlined above for Panel #6 it is expected that "Option #2" would have higher loads due to the larger loading footprint and larger stresses. Table 10 shows the results: as expected, shifting upwind does increase the load on the panel as well as the maximum principal stresses seen in the panel face and in the rib. Thus, the impact point chosen ("Option #3) was less severe than Option #2. In both cases fracture of the panel face would be expected. Figures 36-37 show the various results from the "Option #2" RCC Panel #8 calculation. Based on the stress histories, the panel face would be expected to fail.

Effect of Rotation of Foam Impactor Study

As with the foam insulation impact on tile, there was concern about the effect of the foam impactor having a rotational velocity and how that might affect the impact. To explore the effect of rotation, a series of six computations were performed where the foam impactor had a rotational velocity about one of its major axes, either clockwise or counterclockwise, with a frequency of 18 Hz. Figure 38 shows the various foam orientations and defines the clockwise/counter-clockwise orientation for the results table: the axis of rotation is in the center of the foam and is coming directly out of the page. Clockwise and counterclockwise is defined according to these figures.

The computations were performed with the initial alignment of the Orbiter's z-axis (i.e., α=0°, β=0°). The impact speed was 768 ft/s. The impact location was the same as the baseline case in the impact location study, namely the upper left corner case, with the point be 18.7" up from the carrier panel and 0.83" from the 5-6 T-seal. Table 11 shows the maximum values of the load, the maximum principal

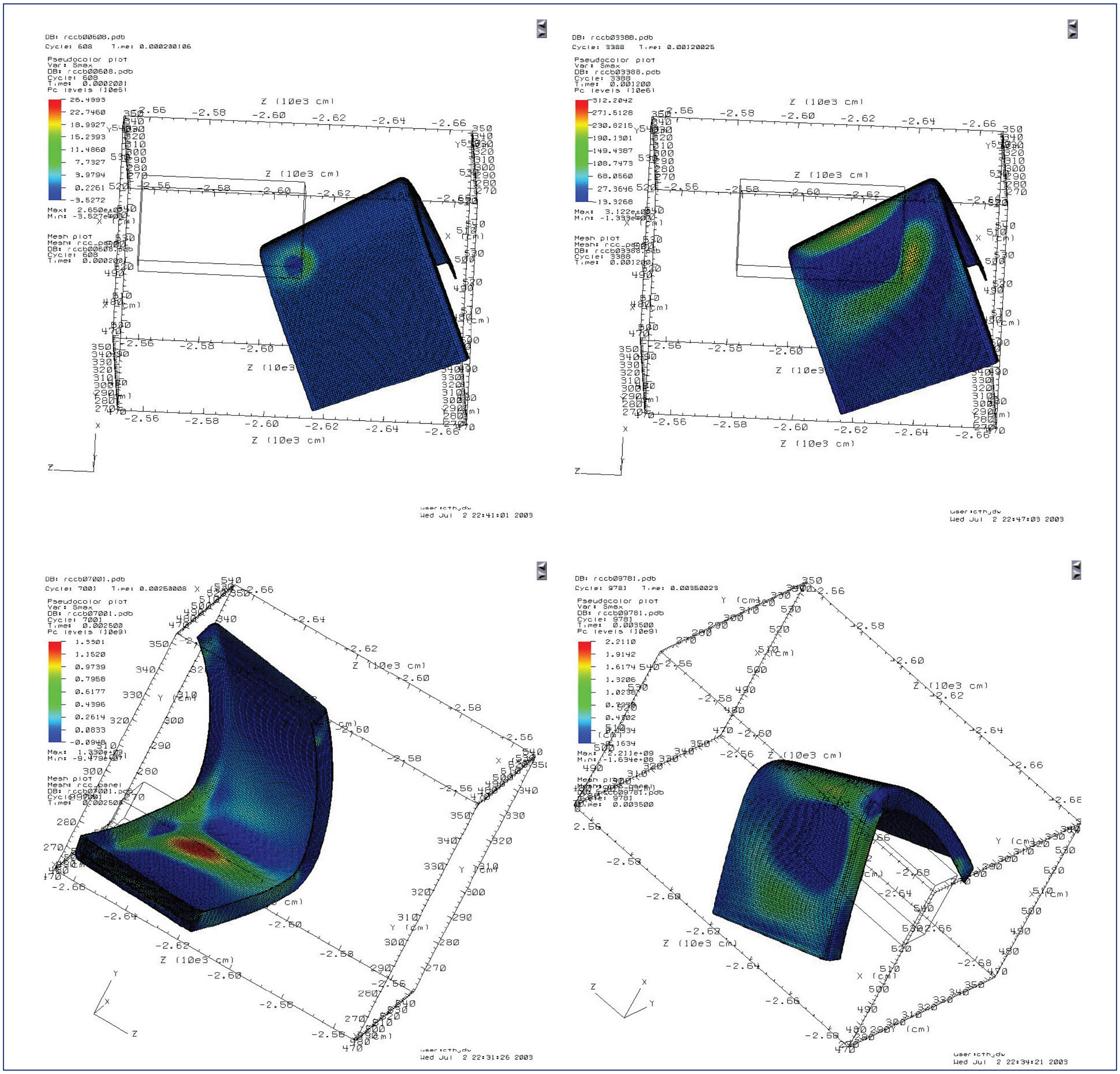

Figure 31. Four frames of the RCC Panel #6 baseline case computation (α=0°, β=0°, 768 ft/s), at 0.2, 1.2, 2.5 and 3.5 ms.

"Option #3" – test condition 25.5" up from carrier panel 7.3" from 7-8 T-seal	Load: 9150 lb (4.07×10⁹ dynes) Panel stress: 43.2 ksi (298 MPa) Rib stress: 33.4 ksi (230 MPa) Displacement: 2.5 in (63 mm) Velocity: 137 ft/s (41.8 m/s)
"Option #2" – not used 25.2" up from carrier panel 4.3" from 7-8 T-seal	Load: 9760 lb (4.34×10⁹ dynes) Panel stress: 48.8 ksi (336 MPa) Rib stress: 35.7 ksi (246 MPa) Displacement: 2.8 in (72 mm) Velocity: 150 ft/s (45.6 m/s)

Table 10. Impact Location Study for RCC Panel #8 (α=5.5°, β=5.0°, 777 ft/s, 30° Clocking Angle).

stress in the panel and the maximum principal stress in the rib over the time from 0 to 5 ms. An immediate conclusion of the computations is that almost all rotational cases lead to larger stresses: only the counterclockwise rotation around the *z*-axis had less load and less stress, but even there, it was not significantly less. Thus, rotation does increase the load delivered to the panel and it increases the stress seen in the panel face and in the rib. The largest load and stresses are seen with the clockwise rotation about the *x*-axis. Stills from this impact are shown in Figure 39, and the various histories are shown in Figs. 40 and 41. The load is increased over the baseline by 32%, the maximum stress in the panel interior by 8% and the maximum principal stress in the rib by 25%. Based on the results of the tests, the rib would be expected to break during this impact.

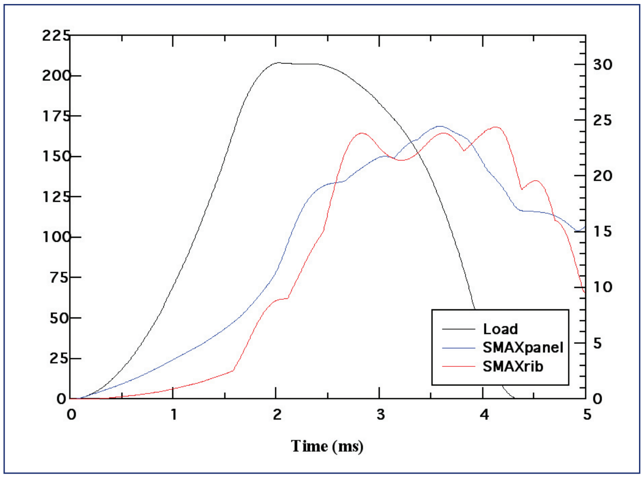

Figure 32. Load and maximum principal stress for panel face and rib vs. time for RCC Panel #6 baseline case computation (α=0°, β=0°, 768 ft/s, 0.83″ from 5-6 T-seal, 18.7″ up from carrier panel).

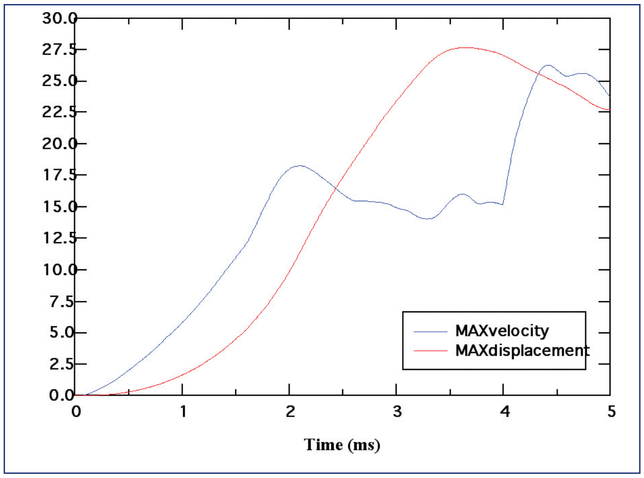

Figure 33. Maximum velocity and maximum displacement vs. time for RCC Panel #6 baseline case computation (α=0°, β=0°, 768 ft/s, 0.83″ from 5-6 T-seal, 18.7″ up from carrier panel).

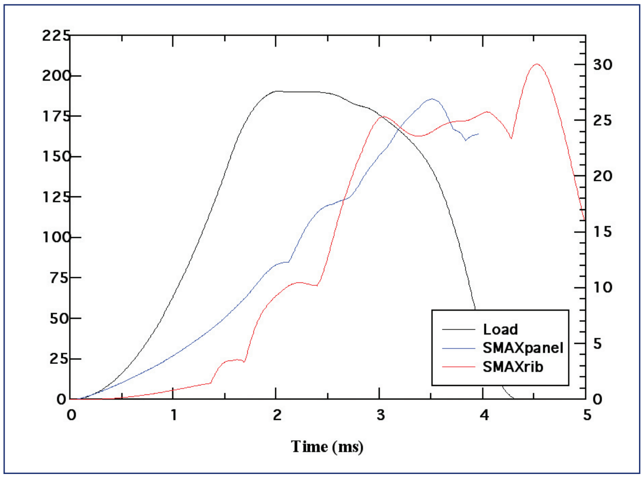

Figure 34. Load and maximum principal stress for panel face and rib vs. time for RCC Panel #6 hit location study maximum stress case (α=0°, β=0°, 768 ft/s, 0.83″ from 5-6 T-seal, 12.7″ from carrier panel).

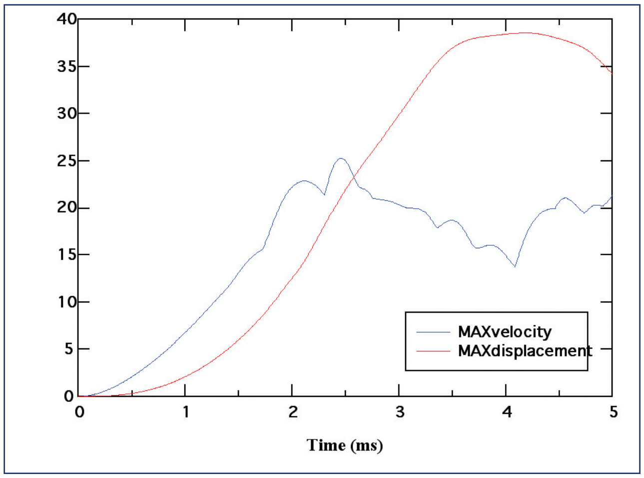

Figure 35. Maximum velocity and displacement vs. time for RCC Panel #6 hit location study maximum stress case (α=0°, β=0°, 768 ft/s, 0.83″ from 5-6 T-seal, 12.7″ up from carrier panel).

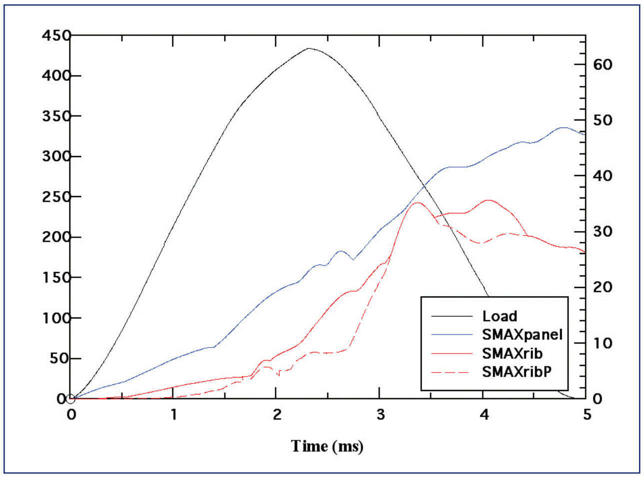

Figure 36. Load and maximum principal stress for panel face and rib vs. time for RCC Panel #8 "Option #2" (α=5.5°, β=5.0°, 777 ft/s).

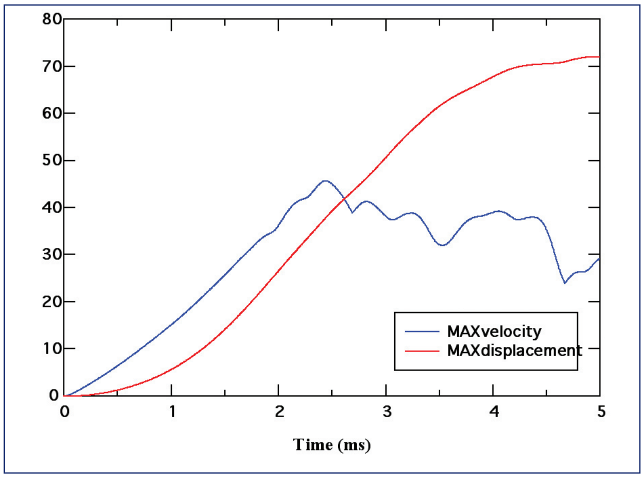

Figure 37. Maximum velocity and displacement vs. time for RCC Panel #8 "Option #2" (α=5.5°, β=5.0°, 777 ft/s).

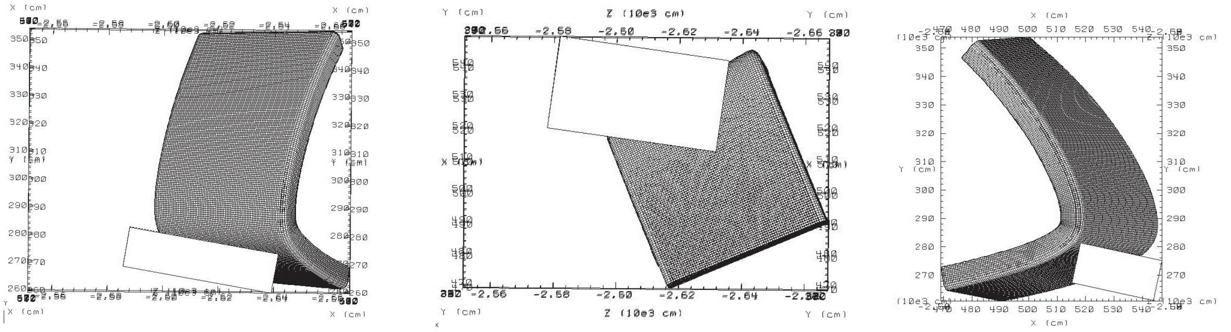

x-axis (from side of Orbiter, looking directly into center).

y-axis (from bottom to top of Orbiter).

z-axis (from front of Orbiter to back).

Figure 38. The three major axes of the foam impactor in Wing Coordinates. The rotational axis is in the geometric center of the presented face of the foam impactor and is coming out of the page. Rotation direction, clockwise and counterclockwise, are defined by these figures (looking down).

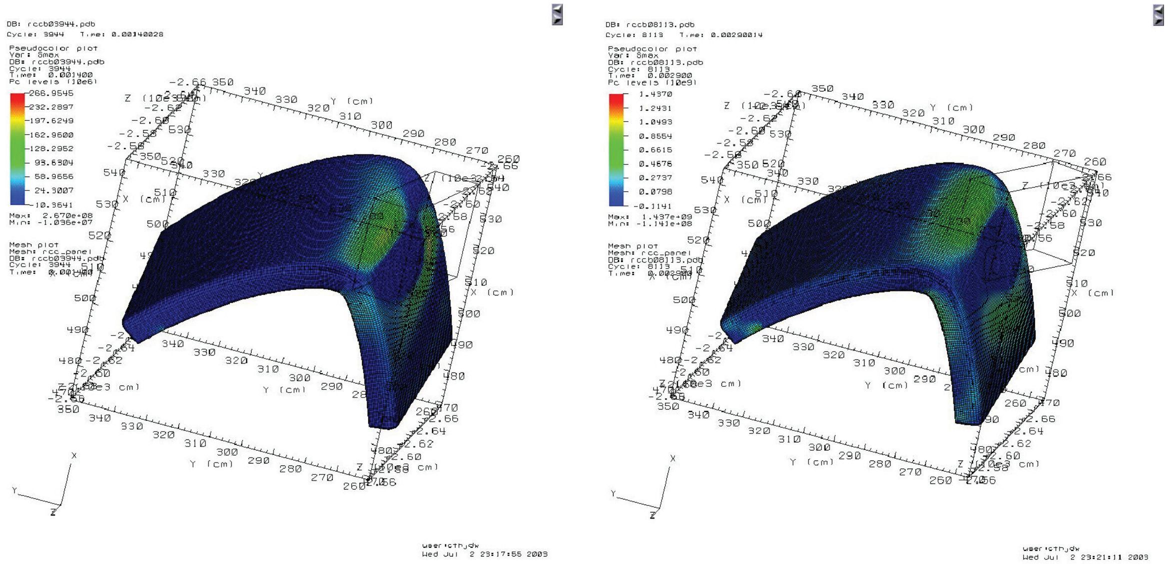

Figure 39. Two frames of the RCC Panel #6 clockwise rotation about x-axis case computation (α=0°, β=0°, 768 ft/s, 18 Hz), at 1.6 (left) and 2.9 (right) ms.

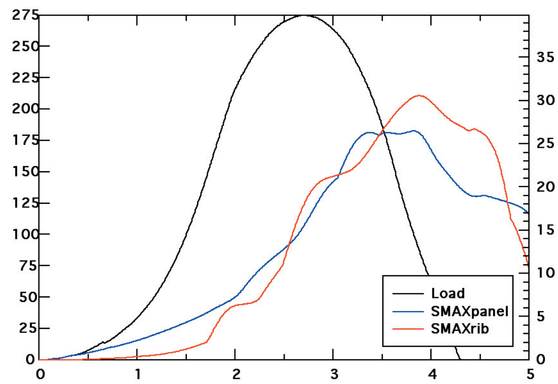

Figure 40. Load and maximum principal stress for panel face and rib vs. time for RCC Panel #6 clockwise rotation about x-axis case (α=0°, β=0°, 768 ft/s, 18 Hz).

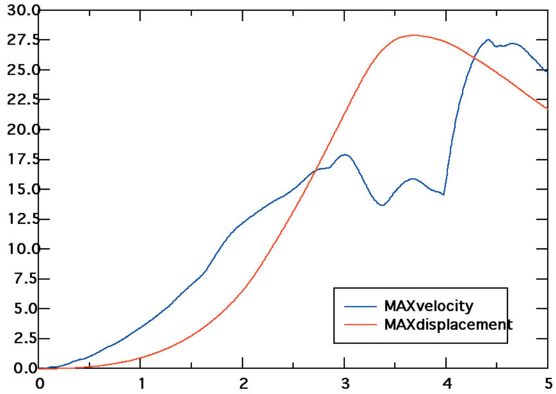

Figure 41. Maximum velocity and displacement vs. time for RCC Panel #6 clockwise rotation about x-axis case (α=0°, β=0°, 768 ft/s, 18 Hz).

Combination of Impactor Rotation and Impact Location

What would be the result of combining the lower impact location with the foam impactor rotation that led to the highest stresses (clockwise about the x-axis)? When these two states were combined, the resulting impact produced even larger loads and stresses as is seen in Table 12 (all save the lower right hand corner have appeared in previous tables). The increase in load over the baseline is 39% and the increase in the stress in the panel face is 36% and in the rib is 61%. Figure 42 shows two stills from the computation, and Figs. 43 and 44 show the various histories. Based on the stress history, it is expected that the panel face would fail.

Axis	*Clockwise*	*Counterclockwise*
x	Load: 6180 lb Panel stress: 26.5 ksi Rib stress: 30.6 ksi	Load: 5380 lb Panel stress: 24.0 ksi Rib stress: 27.6 ksi
y	Load: 4730 lb Panel stress: 24.6 ksi Rib stress: 26.1 ksi	Load: 4890 lb Panel stress: 26.0 ksi Rib stress: 28.8 ksi
z	Load: 5080 lb Panel stress: 26.3 ksi Rib stress: 26.0 ksi	Load: 4250 lb Panel stress: 21.6 ksi Rib stress: 24.4 ksi

Table 11. Results for Rotations about Various Axes. (RCC Panel #6, Baseline Impact Location, α=0°, β=0°, 768 ft/s, 18 Hz Rotation Rate).

Influence of Impact Angle: Increasing α

To study the effect of increasing the impact angle, two additional computations were performed where the angle α was altered. Increasing α increases the angle at which the foam impact strikes the underside of the leading edge: thus, increasing α increases the load delivered to the panel. The results of these computations are shown in Table 13. The table also includes two previous computations for comparison, namely the α=0°, β=0° case that is the baseline for the parameter studies above as well as the actual impact test condition case, where α=5.5°, β=2.5°. All impacts were at 768 ft/s. The impact point for all four was 18.7" above the carrier panel and 0.83" downwind from the 5-6 T-seal. As can be seen from the table, increasing α from 0° to 5.5° increased the load by 35%, increased the panel face stress by 17% and increased the rib stress by 26%. These changes are similar to those produced by the *x*-axis clockwise rotation case, which was the worst case in terms of increasing maximum principal stress in the rib and panel interior. Though not everything is the same, it appears that increasing the impact angle by increasing α on the order of 5° is a reasonable approach to experimentally adjusting for the rotating impactor. A detailed match as was produced for the rotating impact against tile would require a damage model for the RCC, so that the failure process could be matched, as loads are affected by failure, when it occurs and how it progresses.

	No Rotation	*18 Hz Rotation – Clockwise about x-axis*
Baseline impact location 18.7" up from carrier panel 0.83" right of 5-6 T-seal	Load: 4680 lb Panel stress: 24.5 ksi Rib stress: 24.4 ksi	Load: 6180 lb Panel stress: 26.5 ksi Rib stress: 30.6 ksi
Lower impact location 12.7" up from carrier panel 0.83" right of 5-6 T-seal	Load: 4290 lb Panel stress: 26.9 ksi Rib stress: 30.1 ksi	Load: 6510 lb Panel stress: 33.3 ksi Rib stress: 39.3 ksi

Table 12. Combining Most Severe Impact Location and Impactor Rotation (RCC Panel #6, α=0°, β=0°, 768 ft/s).

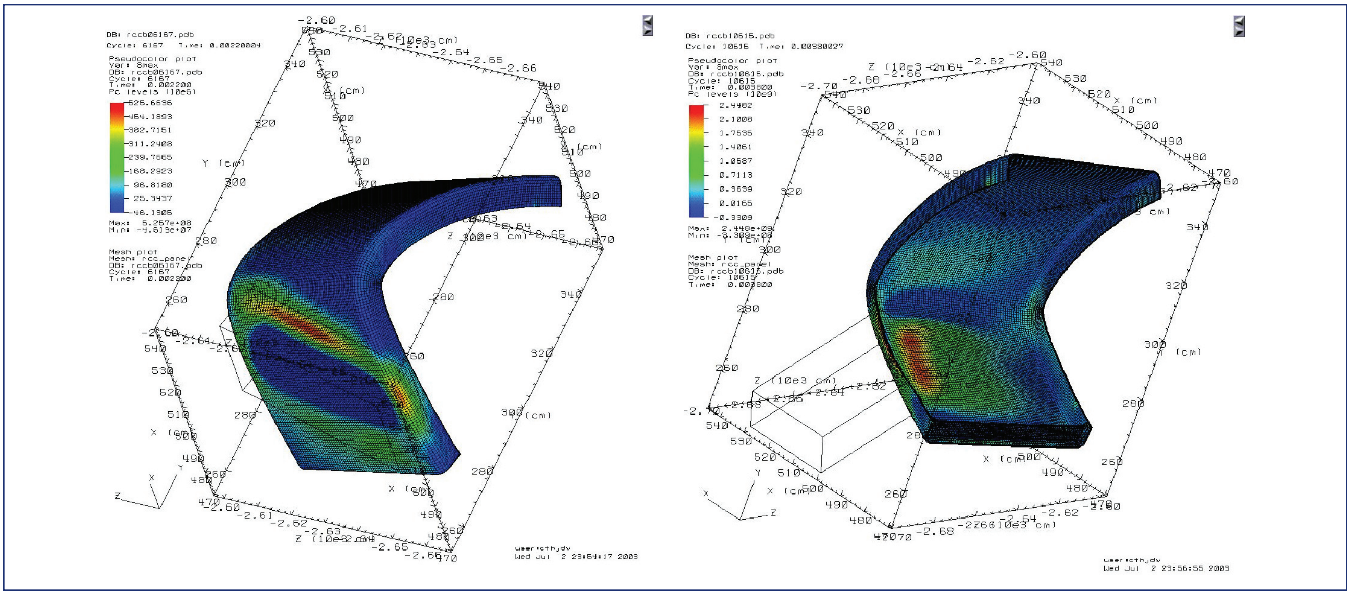

Figure 42. 18 Hz clockwise rotation about x-axis with lower impact point, maximum principal stress at 2.2 (left) and 3.8 (right) ms.

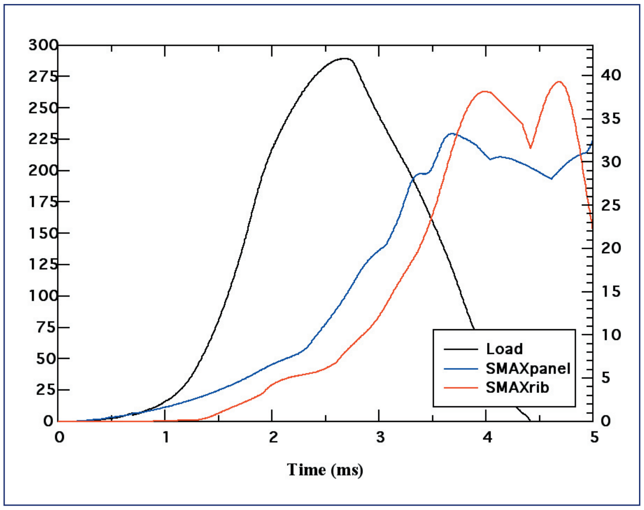

Figure 43. Load and maximum principal stress for panel face and rib vs. time for RCC Panel #6 lower impact point with clockwise rotation about x-axis case (α=0°, β=0°, 768 ft/s, 18 Hz).

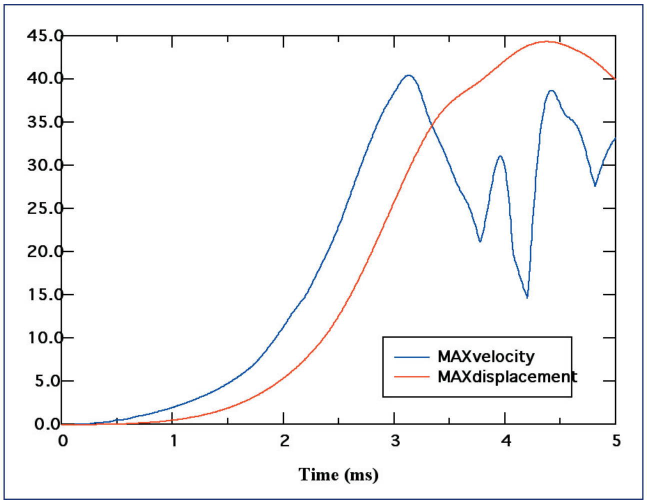

Figure 44. Maximum velocity and displacement vs. time for RCC Panel #6 lower impact point with clockwise rotation about x-axis case (α=0°, β=0°, 768 ft/s, 18 Hz).

α	β	
0°	0°	Load: 4680 lb Panel stress: 24.5 ksi Rib stress: 24.4 ksi
2.25°	0°	Load: 5340 lb Panel stress: 25.9 ksi Rib stress: 26.8 ksi
5.5°	0°	Load: 6300 lb Panel stress: 28.6 ksi Rib stress: 30.7 ksi
5.5°	2.5°	Load: 5850 lb Panel stress: 26.8 ksi Rib stress: 29.2 ksi

Table 13. Results of Various Impact Angle Calculations (RCC Panel #6, Baseline Impact Location, 768 ft/s).

Summary of RCC Computations

Table 14 on the next page summarizes the RCC Panel computations.

Summary

Impact modeling in support of the Columbia Accident Investigation has been performed. It has been shown that for foam insulation impacts, the most important parameter is the component of the velocity vector that is normal to the surface being impacted. This realization allowed the development of a theoretical damage/no damage transition curve for foam insulation impacts against thermal tile. This theoretical curve agreed extremely well with large-scale numerical simulations and with experimental results. During the course of the modeling an equation of state for both the foam insulation and the thermal tiles was developed for the hydrocde CTH. These models gave excellent agreement with data and allowed computations of impacts and calculations of craters with the CTH code. The model was used to analyze the role of impactor rotational velocity, and to arrive at an equivalent impactor that could be more easily launched from the gas gun.

Foam insulation impacts on two of the RCC panels were also modeled (#6 and #8). An analytic boundary condition was developed for the foam impact on the panel. The panels were modeled as elastic, and interpretation of the stress histories was obtained by analyzing the two test cases. Further, parameter studies were carried out on RCC Panel #6 that showed that the upwind, lower on the panel face impacts were the most severe. Impact of foam impactors with rotational velocity against RCC panels was computationally analyzed. Almost all rotational states led to larger stresses in the panel face and rib. It was shown that the most severe 18 Hz rotation could be approximately modeled by increasing the α angle by roughly 5°. Thus result depends strongly on the specific impact geometry.

All in all the modeling was very successful and gave insight into the damage and failure process of thermal tiles and RCC panels under impact by foam insulation.

Acknowledgments

The author wishes to thank Art Nicholls (SwRI) for performing the compression tests on the foam and tile specimens, Erick Sagebiel and Doug McKee (both SwRI) for their assistance with the Pro-E and IGS files for the production of the RCC panel meshes, Don Grosch (SwRI) and Justin Kerr (NASA JSC) for comments, answering questions and providing information about the test geometries and conditions, and Paul Wilde (CAIB) for support and assistance.

Run #	Panel #	Impact Velocity (ft/s)	α	β	Clocking Angle	Rotation Rate (Hz)	Rotation Axis	Impact Point from Carrier Panel	Impact Point from T-seal
4	6	768	0°	0°				18.7″	0.83″
5	6	768	0°	0°				15.7″	0.83″
6	6	768	0°	0°				12.7″	0.83″
7	6	768	0°	0°				18.7″	3.83″
8	6	768	0°	0°				15.7″	3.83″
9	6	768	0°	0°				12.7″	3.83″
10	6	768	0°	0°				18.7″	6.83″
11	6	768	0°	0°				15.7″	6.83″
12	6	768	0°	0°				12.7″	6.83″
13	6	768	0°	0°		+18 (-)	x-axis	18.7″	0.83″
14	6	768	0°	0°		+18 (+)	y-axis	18.7″	0.83″
15	6	768	0°	0°		+18 (-)	z-axis	18.7″	0.83″
16	6	768	0°	0°		-18 (+)	x-axis	18.7″	0.83″
17	6	768	0°	0°		-18 (-)	y-axis	18.7″	0.83″
18	6	768	0°	0°		-18 (+)	z-axis	18.7″	0.83″
19	6	768	0°	0°		-18 (+)	x-axis	12.7″	0.83″
23	6	768	5.5°	2.5°				18.7″	0.83″
25	6	768	2.25°	0°				18.7″	0.83″
26	6	768	5.5°	0°				18.7″	0.83″
24	8	777	5.5°	5°	30°			25.2″	4.3″
27	8	777	5.5°	5°	30°			25.5″	7.3″

Table 14. Summary of RCC Panel Computations Discussed in This Report. For Rotation Rate, the leading sign is the actual sign of the component of the rotation vector; a parenthetical + sign means clockwise with respect to Figure 38 and a parenthetical - sign means counterclockwise with respect to Figure 38.

References For Appendix D.12

1. Drew L. Goodlin, "Orbiter Tile Impact Testing," Southwest Research Institute Final Report #18-7503-005 prepared for NASA JSC, San Antonio, Texas, March 5, 1999.
2. J. M. McGlaun, S. L. Thompson and M. G. Elrick, "CTH: A Three-Dimensional Shock Wave Physics Code," *International Journal Impact Engineering*, Vol. 10, pp. 351-360, 1990.
3. D. J. Grosch and J. P. Riegel, III, "Ballistic Testing of Orbiter Tiles," Southwest Research Institute Final Report #06-2720 prepared for Rockwell International, San Antonio, Texas, February 10, 1989.
4. Mark L. Wilkins, *Computer Simulation of Dynamic Phenomena*, Springer-Verlag, Berlin, 1999.

Footnotes For Appendix D.12

[*] All computations in this report were carried out in the metric system, in cgs. However, due to the prevalent use of English units in the Shuttle program, many of the results will be presented in English units or both systems.

[*] This data is included for completeness; the damage/no damage transition curve would be different for this material – see the discussion below on the effects of increasing foam density.